

Analysis of isothermal and cooling rate dependent immersion freezing by a unifying stochastic ice nucleation model

P. A. Alpert^{1,*} and D. A. Knopf¹

¹Institute for Terrestrial and Planetary Atmospheres/School of Marine and Atmospheric Sciences, Stony Brook University, Stony Brook, NY 11794-5000, USA

* now at: Institut de Recherches sur la Catalyse et l'Environnement de Lyon, Centre National de la Recherche Scientifique, Université Claude Bernard Lyon 1, 69626 Villeurbanne, France

Correspondence to: P. A. Alpert (peter.alpert@ircelyon.univ-lyon1.fr) and D. A. Knopf (daniel.knopf@stonybrook.edu)

Abstract. Immersion freezing is an important ice nucleation pathway involved in the formation of cirrus and mixed-phase clouds. Laboratory immersion freezing experiments are necessary to determine the range in temperature (T) and relative humidity (RH) at which ice nucleation occurs and to quantify the associated nucleation kinetics. Typically, isothermal (applying a constant temperature) and cooling rate dependent immersion freezing experiments are conducted. In these experiments it is usually assumed that the droplets containing ice nuclei (IN) all have the same IN surface area (ISA), however the validity of this assumption or the impact it may have on analysis and interpretation of the experimental data is rarely questioned. A stochastic immersion freezing model based on first principles of statistics is presented, which accounts for variable ISA per droplet and uses physically observable parameters including the total number of droplets (N_{tot}) and the heterogeneous ice nucleation rate coefficient, $J_{\text{het}}(T)$. This model is applied to address if (i) a time and ISA dependent stochastic immersion freezing process can explain laboratory immersion freezing data for different experimental methods and (ii) the assumption that all droplets contain identical ISA is a valid conjecture with subsequent consequences for analysis and interpretation of immersion freezing.

The simple stochastic model can reproduce the observed time and surface area dependence in immersion freezing experiments for a variety of methods such as: droplets on a cold-stage exposed to air or surrounded by an oil matrix, wind and acoustically levitated droplets, droplets in a continuous flow diffusion chamber (CFDC), the Leipzig aerosol cloud interaction simulator (LACIS), and the aerosol interaction and dynamics in the atmosphere (AIDA) cloud chamber. Observed time dependent isothermal frozen fractions exhibiting non-exponential behavior with time can be readily explained by this model considering varying ISA. An apparent cooling rate dependence of J_{het} is ex-

plained by assuming identical ISA in each droplet. When accounting for ISA variability, the cooling rate dependence of ice nucleation kinetics vanishes as expected from classical nucleation theory. The model simulations allow for a quantitative experimental uncertainty analysis for parameters N_{tot} , T ,
25 RH, and the ISA variability. In an idealized cloud parcel model applying variability in ISAs for each droplet, the model predicts enhanced immersion freezing temperatures and greater ice crystal production compared to a case when ISAs are uniform in each droplet. The implications of our results for experimental analysis and interpretation of the immersion freezing process are discussed.

1 Introduction

30 Ice crystals in tropospheric clouds form at altitudes where temperatures fall below the ice melting point, also known as supercooled temperatures, and for conditions in which water partial pressure exceeds the saturation vapor pressure with respect to ice (Pruppacher and Klett, 1997; Hegg and Baker, 2009). Cirrus or mixed-phase clouds consist entirely of ice crystals or of ice crystals coexisting with supercooled aqueous droplets, respectively. These clouds can significantly impact the global radiative budget and the hydrological cycle (Baker, 1997; Rossow and Schiffer, 1999; Chen et al., 2000; 35 Liu et al., 2007; Lohmann and Hoose, 2009; Tao et al., 2012; Rosenfeld et al., 2014), however, their formation is not well understood or constrained in cloud and climate models (Boucher et al., 2013). Ice nucleation precedes the formation of ice crystals. Homogeneous ice nucleation occurs from supercooled aqueous aerosol particles or cloud droplets. Ice formation can also occur at temperatures 40 higher than the homogeneous freezing limit initiated by insoluble particles acting as ice nuclei (IN). Heterogeneous ice nucleation can occur when IN are immersed in supercooled aqueous droplets, termed immersion freezing, when IN make physical contact with supercooled droplets, termed contact freezing, or when ice nucleates on IN directly from the supersaturated vapor phase, termed deposition ice nucleation. It is impossible to observe in situ ice nucleation in the atmosphere and 45 very difficult to infer the ice nucleation pathway (Haag et al., 2003; Hegg and Baker, 2009). Despite the established importance of the impact of heterogeneous ice nucleation on cirrus and mixed-phase cloud formation, it is not included in global radiative forcing estimates (Myhre et al., 2013).

Laboratory studies are necessary to investigate at which thermodynamic conditions, i.e. temperature, T , and relative humidity, RH, and by which mode ice nucleation occurs for predictive use in 50 cloud and climate models. This study presents a newly developed model simulation applied for analyses of previously published laboratory immersion freezing data obtained by different experimental methodologies. It allows prediction of atmospheric ice particle production under relevant scales of time and IN surface area (ISA).

Classical Nucleation Theory (CNT) is currently the only available physical theory to describe ice 55 nucleation. Simply stated, CNT quantifies a maximum Gibbs free energy barrier corresponding to the minimum number of water molecules in a cluster that has to be overcome to initiate ice nucleation

(Pruppacher and Klett, 1997). Cluster formation and thus, ice nucleation, occurs stochastically and is dependent on time, t , and in the case of homogeneous ice nucleation, the supercooled liquid volume, V . Koop et al. (2000) parameterized the theoretical homogeneous ice nucleation rate coefficient, J_{hom} , as a function of T and water activity, a_w ($a_w = 1.0$ for pure water and $a_w < 1.0$ for aqueous solution). This approach yields J_{hom} to be independent of the nature of the solute and avoids the weakness of the capillary approximation in CNT (Pruppacher and Klett, 1997).

Immersion freezing can be described by CNT by reducing the free energy barrier due to the presence of a solid surface. Ice nucleation remains a stochastic process, but is dependent on the available ice nucleating surface area, A , instead of V (Pruppacher and Klett, 1997; Zobrist et al., 2007). The heterogeneous ice nucleation rate coefficient, J_{het} , is a physically and experimentally defined parameter which gives the rate of nucleation events for given surface area and unit time. Knopf and Alpert (2013) parameterized J_{het} as a function of T and a_w following Koop et al. (2000) using direct measurements of J_{het} and J_{het} derived from previous studies (Archuleta et al., 2005; Alpert et al., 2011a, b; Knopf and Forrester, 2011; Murray et al., 2011; Broadley et al., 2012; Iannone et al., 2011; Pinti et al., 2012; Rigg et al., 2013). Known as the a_w based immersion freezing model (ABIFM) (Knopf and Alpert, 2013), J_{het} can be derived for different types of IN such as mineral dusts, organic, surfactant and biogenic, applicable for $a_w \leq 1.0$, and independent of the nature of the solute. The ABIFM is a holistic and computationally efficient physical description of the immersion freezing process for prediction of ice nucleation for atmospherically relevant conditions and applicable for a variety of experimental methods, including the droplet-on-substrate approach (Zobrist et al., 2007; Knopf and Forrester, 2011; Alpert et al., 2011a, b; Iannone et al., 2011; Murray et al., 2011; Broadley et al., 2012; Rigg et al., 2013), oil-encased droplets (Murray et al., 2011; Broadley et al., 2012; Wright and Petters, 2013), differential scanning calorimetry (Marcolli et al., 2007; Pinti et al., 2012), and continuous flow diffusion (Rogers et al., 2001; Archuleta et al., 2005; Hartmann et al., 2011; Kulkarni et al., 2012; Wex et al., 2014). These previous studies represent a subset of a much broader selection of experimental methods and designs.

The major difficulty with a variety of experimental techniques is how accuracy and uncertainty of T , RH, t , and A are assessed and how these uncertainties affect extrapolation of laboratory derived ice nucleation parameterizations to atmospherically relevant conditions. Previous investigations have developed state of the art instrumentation and methods to constrain uncertainties (Connolly et al., 2009; Lüönd et al., 2010; Niedermeier et al., 2010; DeMott et al., 2010; Niedermeier et al., 2011; Hoose and Möhler, 2012; Niemand et al., 2012; Rigg et al., 2013; Hiranuma et al., 2015; Vali and Snider, 2015). However, interpreting ice nucleation using non-physical (or empirical) parameterizations or models that are fitted to measured frozen fractions and ice crystal concentrations are inherently constrained to the investigated range of T , RH, t , and A and concentration of INPs (Rigg et al., 2013; Knopf and Alpert, 2013). These include the multi-component model (Murray et al., 2011), the time-dependent freezing rate parcel model (Vali and Snider, 2015), parameterizations of IN per

liter of air (DeMott et al., 2010), the α -PDF model (Marcolli et al., 2007; Lüönd et al., 2010), the
95 active site model (Marcolli et al., 2007; Lüönd et al., 2010), the singular description (Vali, 1971;
Connolly et al., 2009; Alpert et al., 2011a, b; Vali, 2008; Murray et al., 2011; Hiranuma et al., 2015)
and the soccer ball model (Niedermeier et al., 2011). For example, Rigg et al. (2013) showed that the
single contact angle model, α -PDF model, active site model and singular description cannot describe
the freezing point depression (e.g. Zuberi et al., 2002; Archuleta et al., 2005; Koop and Zobrist,
100 2009) and nucleation kinetics (in analogy of homogeneous ice nucleation) observed in immersion
freezing experiments where the IN are immersed in aqueous solution droplets (Rigg et al., 2013;
Knopf and Alpert, 2013). surface. According to the singular hypothesis, the number of active sites,
 $n_s(T)$, is dependent on T only and neglects ice nucleation kinetics. Wex et al. (2014) parameterized
 f_{frz} data accounting for the freezing point depression using a temperature offset approach follow-
105 ing Koop and Zobrist (2009) and using a singular description, i.e. deriving $n_s(T, a_w)$. However, the
approach the authors used is solute type dependent (Koop and Zobrist, 2009) and thus, may be cum-
bersome for atmospheric application where INPs can be associated with a wide variety of solutes.
These limitations clearly support further analytical efforts to improve our understanding on the gov-
erning parameters of immersion freezing.

110 The immersed ISA per droplet is important for experimental derivation of J_{het} and for deriving
empirical quantities such as $n_s(T)$ or other fitting functions and their parameters. In previous exper-
imental studies, droplets for ice nucleation experiments were dispensed from a bulk solution con-
taining IN (Broadley et al., 2012; Rigg et al., 2013; Wright and Petters, 2013; Herbert et al., 2014;
Diehl et al., 2014). In other investigations, solid particles were size selected by their electrical mobil-
115 ity and then injected into, or continuously flown through, an ice nucleation chamber where water con-
densation precedes ice nucleation (Archuleta et al., 2005; Niedermeier et al., 2010; Kulkarni et al.,
2012; Welti et al., 2012; Wex et al., 2014). In these studies and those that used polydisperse aerosol
(e.g. Niemand et al., 2012), surface area calculations assumed that particles with the same mobility
diameter are spherical with identical surface area. Despite this assumption, advancement in account-
120 ing for particle size variability considering multiple charged particles in ice nucleation experiments
has been made (Lüönd et al., 2010; Augustin-Bauditz et al., 2014). However, extensive theoretical
and experimental literature exists on aerosol sizing instrumentation and morphology characteriza-
tion, which consider particle density, void fraction, shape and electrical charge effects implying their
non-sphericity (DeCarlo et al., 2004; Slowik et al., 2004; Zelenyuk et al., 2006; Schmid et al., 2007;
125 Park et al., 2008). In general, neglecting these effects likely influences surface area estimates. Also,
distributions of immersed ISA per droplet are typically assumed to be monodispersed, or in other
words, each droplet is assumed to contain identical ISA. Furthermore, the number of droplets ap-
plied in an ice nucleation experiment may also affect the significance of the freezing data and thus
interpretation of the experiment. It is necessary to question if a potential variability in ISA and/or
130 the assumption of monodispersed ISA and a limited number of observed freezing events become im-

portant for interpretation of immersion freezing experiments with subsequent ramifications for the analytical ice nucleation description.

We introduce a newly developed model simulation in which ice nucleation is treated explicitly as a stochastic process applicable for isothermal and cooling rate experiments. Previous experimental results using different experimental methods are simulated and compared for a wide range of atmospherically relevant conditions. Sensitivity studies on frozen fraction data and experimentally derived J_{het} are performed as a function of ISA assumptions, the number of droplets employed in the experiment, T , and RH. The validity of typical assumptions of ISA variability and uncertainty are tested. Then, a detailed analysis of the ability of the model simulation to reproduce experimental results with strict uncertainty estimation is presented for 7 independent immersion freezing studies utilizing 8 different instrumentation: (i) droplets on a cold-stage exposed to air, (ii) droplets on a cold-stage covered in oil, (iii) oil-droplet emulsions, (iv) droplet acoustic levitation, (v) droplet wind tunnel levitation, (vi) the Leipzig aerosol cloud interaction simulator (LACIS), (vii) a continuous-flow diffusion chamber (CFDC) and (viii) the aerosol interaction and dynamics in the atmosphere (AIDA) cloud chamber. A rigorous uncertainty analysis of the ice nucleation kinetics for typical ranges in experimental conditions is presented. The atmospheric implications by application of a simple cloud model are discussed.

2 Immersion freezing model based on classical nucleation theory

2.1 Simulation of isothermal freezing experiments

Stochastic immersion freezing simulations (IFSs) are performed to evaluate the effect of variable ISA on droplet immersion freezing experiments conducted in the laboratory. As discussed above, different droplets in a laboratory experiment will possess different ISA. To account for this fact, ISA in each simulated droplet is sampled from a lognormal distribution to mimic this variability with the most probable ISA being A_g or a mean distribution parameter $\mu = \ln(A_g)$. The distribution width parameter is $\sigma = \ln(\sigma_g)$, where σ_g represents the factor by which ISA can vary. Knowledge of ISA for each droplet can be directly used as an alternative without a need for random sampling. Droplet freezing for isothermal experiments can then be described by

$$\delta N_{\text{ufz}} = -J_{\text{het}} A_{\text{tot}} \delta t, \quad (1)$$

where δN_{ufz} represents the change in the number of unfrozen droplets after a certain interval of time, δt , and J_{het} is the heterogeneous ice nucleation rate coefficient. The total available ISA is $A_{\text{tot}} = \sum A_j$, where A_j is the ISA in the j th droplet. An assumption typically made is that all droplets contain the same ISA, or $A_{\text{tot}} = A_g N_{\text{ufz}}$, where A_g is the ISA for all droplets (e.g. Marcolli et al., 2007; Lüönd et al., 2010; Niedermeier et al., 2010; Murray et al., 2011; Rigg et al., 2013). Using

this assumption and assuming a continuous differential in Eq. (1) leads to,

$$165 \quad \frac{dN_{\text{ufz}}}{N_{\text{ufz}}} = -J_{\text{het}} A_g dt, \quad (2)$$

Integrating Eq. (2) further results in the commonly used expression for the fraction of frozen droplets,

$$f_{\text{frz}} = \frac{N_{\text{frz}}}{N_{\text{tot}}} = 1 - e^{-J_{\text{het}} A_g t}, \quad (3)$$

The form of the expression given in Eq. (3) is used in many studies although modified slightly when considering multiple components or contact angle distributions (e.g. Niedermeier et al., 2010; Murray et al., 2011; Broadley et al., 2012; Rigg et al., 2013), and when particle or droplet sizes are discretized or binned (e.g. Marcolli et al., 2007; Lüönd et al., 2010). The major weakness of this exponential form to describe f_{frz} lies entirely in the assumption it is based on, i.e. it is only valid if the ISA is exactly the same for all droplets considered. When taking into account individual droplet ISA for all droplets, this formulation is not valid. Thus, application of this formula to interpret ice nucleation studies, or use in mathematical frameworks, strictly speaking, is also invalid when ISA on a droplet per droplet basis is different.

The ISA in a single droplet is a measurable quantity with a corresponding measurement uncertainty. It is unlikely that every droplet prepared in an immersion freezing experiment has identical ISA. For the same particle type, there will exist a systematic ISA uncertainty with respect to a particular droplet preparation technique. This systematic uncertainty is σ_g and can be determined by directly measuring ISA in a population of independently prepared droplets. Since the ISA variability is not resolved in previous experiments, a droplet freezing simulation must be employed to model ice nucleation for interpretation purposes. To accomplish this, freezing of each single droplet is assumed to be stochastic, or in other words, there exists a probability of the j th droplet to freeze, $P_{j,\text{frz}}$, within δt . The probability for a single droplet not to freeze, $P_{j,\text{ufz}}$, is realized as an exponential decay law (Pruppacher and Klett, 1997; Koop et al., 1997) and therefore,

$$P_{j,\text{frz}} = 1 - P_{j,\text{ufz}} = 1 - e^{-J_{\text{het}} A_j \delta t}. \quad (4)$$

We apply a time and surface area dependent immersion freezing process which follows CNT and therefore, all simulations employ J_{het} having units of $\text{cm}^{-2} \text{s}^{-1}$. However, J_{het} does not explicitly depend on time and ISA, but on T and a_w . A droplet can either remain in an unfrozen state or freeze and therefore, is described exactly by a binomial distribution, $B(k; n, P_{j,\text{frz}})$, with parameters $P_{j,\text{frz}}$ given by Eq. (4) and $n = 1$ meaning that only one trial is given for an individual droplet to freeze in δt . A randomly sampled number, $k = 0$ or 1 , is obtained from the distribution

$$B(k; n = 1, P_{j,\text{frz}}) = P_{j,\text{frz}}^k (1 - P_{j,\text{frz}})^{1-k} \quad (5)$$

for each droplet with a normalization prefactor, $n!/(k!(n-k)!) = 1$. When $k = 1$, freezing occurs for the j th droplet and if $k = 0$, the droplet does not freeze and another k is sampled in the next time

interval. For a collection of multiple droplets, the number of freezing events that occur in a given time interval is n_{frz} and the cumulative sum as a function of time is $N_{\text{frz}}(t)$. For a single IFS starting with N_{tot} liquid droplets, the fraction of unfrozen droplets is $f_{\text{ufz}}(t) = 1 - N_{\text{frz}}(t)/N_{\text{tot}}$.

200 A record of n_{frz} and corresponding droplet ISA, i.e. A_j , is kept for a single IFS. This record can be thought of as a simulated experimental immersion freezing data set, i.e. it gives a record of droplet freezing time while tracking A_j . Due to the stochastic nature of nucleation, repetition of isothermal IFSs will not result in identical values of f_{ufz} over t . Likewise, repetition of a laboratory experiment will not result in exactly the same $f_{\text{ufz}}(t)$ curve. Therefore it is necessary to repeat the simulations in order to reveal a range of $f_{\text{ufz}}(t)$ values of which the mean unfrozen fraction, $\bar{f}_{\text{ufz}}(t)$, can be derived 205 from all simulations. We choose an ensemble of 10^5 IFSs to accurately determine $\bar{f}_{\text{ufz}}(t)$. This procedure is a basic form of a Monte Carlo method and yields upper and lower percentile bounds at 5 and 95% serving as a stochastic uncertainty of the immersion freezing process. We define stochastic uncertainty as the scatter in the data due to the occurrence of random (i.e. stochastic) freezing events 210 upon repeat experiments as a result of a set number of observed freezing events.

An ensemble of IFSs, referred to as a model simulation, requires the selection of parameters N_{tot} , A_g , σ_g , and J_{het} . For demonstration purposes, the parameter choice is arbitrary. However, when reproducing a laboratory derived data set, a parameter selection process is applied. Parameters which can be directly accessed from previous laboratory studies are first selected to mimic experimental 215 conditions. For example, if a study reports that 100 droplets were examined in an immersion freezing experiment, then $N_{\text{tot}} = 100$. Some previous studies report only average ISA per droplet, A_{avg} , and neglect information for estimating σ_g . If A_{avg} is reported as $7.1 \times 10^{-6} \text{ cm}^2$, then for simplicity we set $A_g = 7.1 \times 10^{-6} \text{ cm}^2$. For all studies in which a parameter is not available or easily calculated, it is fitted to experimentally derived f_{ufz} or f_{frz} , and critically assessed whether or not the 220 parameter best reproduces experimental conditions. This applies to J_{het} and σ_g , the latter of which is not typically considered in previous studies. In many isothermal immersion freezing laboratory studies, droplet freezing continues over time when all other conditions remain constant, i.e. at constant T (Wright and Petters, 2013; Murray et al., 2011; Broadley et al., 2012; Herbert et al., 2014). Therefore, the J_{het} parameter is selected to be constant for isothermal IFSs.

225 2.2 Simulation of cooling rate dependent immersion freezing experiments

2.2.1 Experimentally derived J_{het} for model input

When a cooling rate is applied in model simulations, droplet freezing is simulated in discrete temperature intervals and therefore J_{het} at every step is required for deriving $P_{j,\text{frz}}$. In this study, only water droplets are considered and therefore, it is assumed that $a_w = 1.0$ and J_{het} becomes a function of T 230 only. Ideally, experimentally derived $J_{\text{het}}(T)$ should be used for prediction of immersion freezing. However, these data sets are usually limited in T range and are discrete in nature. Knopf and Alpert

(2013) compiled experimental data which was parameterized as a continuous function over T following the ABIFM expressed as,

$$\log_{10}(J_{\text{het}}) = m\Delta a_w + c, \quad (6)$$

235 where m and c are slope and intercept parameters, respectively, and Δa_w is the independent variable following the formulation of Koop et al. (2000). The Δa_w at which a droplet freezes is calculated by subtracting the a_w of the droplet (= 1.0 for pure water) from the water activity point that falls on the ice melting curve, $a_{w, \text{ice}}(T)$, at the same temperature or

$$\Delta a_w = a_w(T) - a_{w, \text{ice}}(T), \quad (7)$$

240 where

$$a_{w, \text{ice}}(T) = p_{\text{ice}}(T)/p^{\circ}_{\text{H}_2\text{O}}(T), \quad (8)$$

and $p_{\text{ice}}(T)$ and $p^{\circ}_{\text{H}_2\text{O}}$ are the vapour pressure with respect to planar ice and water, respectively (Murphy and Koop, 2005).

Resulting calculations from Eqs. (6) to (8) are not computationally demanding and conveniently
245 derive $J_{\text{het}}(T)$ for model input. Note that for isothermal model simulations, a continuous function of J_{het} is not required and thus model derived J_{het} is independent from the ABIFM.

2.2.2 Simulated droplet freezing

Cooling rate dependent IFSs are performed to evaluate the effect of stochastic freezing and variable ISA in laboratory immersion freezing experiments. Again, the ISA for a single droplet is sampled
250 from a lognormal distribution, however, Eqs. (1) and (4) are modified to

$$\delta N_{\text{ufz}} = -\frac{A_{\text{tot}}}{r} J_{\text{het}}(T) \delta T, \quad (9)$$

and

$$P_{j, \text{frz}} = 1 - P_{j, \text{ufz}} = 1 - e^{-\frac{A_j}{r} J_{\text{het}}(T) \delta T}, \quad (10)$$

respectively, where δT is a temperature interval and $r = \delta T / \delta t$ is the cooling rate. $J_{\text{het}}(T)$ is calculated from Eq. (6) and used in Eq. (10). Once the probability for the j th droplet to freeze is calculated
255 for all droplets, freezing is determined by sampling from $B(k; n, P_{j, \text{frz}})$ (Eq. 5). The number of freezing events that occur in a given δT is n_{frz} , and the cumulative sum as a function of T is $N_{\text{frz}}(T)$ and used to calculate frozen fractions of droplets, $f_{\text{frz}}(T) = N_{\text{frz}}(T) / N_{\text{tot}}$. Similar to isothermal freezing, a single r dependent IFS yields a droplet immersion freezing record analogous to an experimental
260 data set. In this case, the record of droplet freezing and corresponding A_j is a function of T . The average frozen fraction for 10^5 simulations, $\bar{f}_{\text{frz}}(T)$, is calculated along with percentiles at 5 and 95%, the latter used as a stochastic uncertainty.

It is important to note that application of r dependent IFSs presented here do not require the AB-IFM, as it is only used as a parameterization of previously published immersion freezing data sets to calculate $J_{\text{het}}(T)$. Any other published $J_{\text{het}}(T)$ will work equally as well. The ABIFM parameterization is IN type dependent and suitable for saturated and subsaturated conditions, i.e. $a_w \leq 1$, or $\text{RH} \leq 100\%$, if the droplet is in equilibrium with the water vapor phase. Therefore, the ABIFM is a useful and convenient tool for model input $J_{\text{het}}(T)$.

3 Results and discussion

3.1 Isothermal model simulations of individual droplet freezing experiments

Figure 1a shows 5 and 95% bounds of f_{ufz} from 4 model simulations for different N_{tot} applying either uniformly equal ($\sigma_g = 1$) or lognormally distributed ($\sigma_g = 10$) ISA per droplet as given in Table 1. Two of these test cases, Iso1 and Iso2, have uniform ISA both resulting in f_{ufz} (on a logarithmic scale) linear with t . However, the spread of the 5 and 95% bounds is much wider for Iso2 having $N_{\text{tot}} = 30$ than for Iso1 having $N_{\text{tot}} = 1000$. It is clear that a larger spread in simulated f_{ufz} is entirely due to applied smaller N_{tot} . This implies that a laboratory experiment using a small N_{tot} , is statistically less significant compared to an experiment with greater N_{tot} . A single experimentally derived f_{ufz} curve under the same conditions as Iso2 will fall anywhere between the upper and lower bounds, and thus may even appear to deviate from a log-linear relationship over time. Therefore, interpretation about the nature of the heterogeneous ice nucleation process from the slope of f_{ufz} over time for an experiment using small N_{tot} should be conducted with care.

Model simulations Iso3 and Iso4 are shown in Fig. 1a where $N_{\text{tot}} = 1000$ and 30, respectively, and the ISA per droplet is sampled from lognormal distribution with $\sigma_g = 10$. In Iso3, f_{ufz} significantly deviates from a log-linear relationship with t . In Iso4, the same curvature exists, however the percentile bounds are much wider due to applied smaller N_{tot} . It is important to note that J_{het} is the same and constant for all simulations shown in Fig. 1a. The nucleation rate of each j th droplet can be calculated as, $\omega_{\text{het},j} = J_{\text{het}}A_j$ with units of s^{-1} . The droplets having a larger or smaller ISA will result in larger or smaller $\omega_{\text{het},j}$, respectively. The fact that f_{ufz} is linear for $\sigma_g = 1$, the curvature effect in f_{ufz} seen for $\sigma_g = 10$ must be entirely due to ISA variability. This is because droplets with greater values of $\omega_{\text{het},j}$ will tend to nucleate more rapidly than those having smaller $\omega_{\text{het},j}$ values. In other words, the curvature of $f_{\text{ufz}}(t)$ is entirely due to those droplets having larger and smaller ISA that freeze within shorter and longer time scales, respectively. In addition, the spread in the 5 and 95 percentiles is very similar for Iso1 and Iso3, and for Iso2 and Iso4. This is seen most clearly at the intersection of the blue and green shaded regions ($t \simeq 1.3 \text{ min}$). In isothermal freezing experiments, variability in ISA will not significantly affect stochastic uncertainty estimates, but will cause $f_{\text{ufz}}(t)$ to deviate from a log-linear relationship. From this we can conclude that the effects of droplet numbers and ISA variability on f_{ufz} can be decoupled and independently assessed.

In some previous experimental isothermal immersion freezing studies, the number of liquid droplets and an estimate of the average ISA per droplet are provided or can be derived. However, the validity
300 of the assumption that all droplets possess the same ISA is rarely investigated or quantified. Similarly, J_{het} is not often reported. However, laboratory data do provide an opportunity to test our model for robustness while using parameters similar to those reported in the experimental studies. In fact, our model can also provide estimates for parameters typically unreported or unavailable, such as J_{het} and σ_g .

305 Experimental data by Wright and Petters (2013) for isothermal immersion freezing by Arizona Test Dust (ATD) is very well reproduced by model simulation IsoWR as demonstrated in Fig. 1b. Parameters for IsoWR are given in Table 1 and chosen to mimic experimental conditions in which droplets contained 1 wt % ATD held at 251 K. Bounds at 5 and 95 % of simulated f_{ufz} are shown in Fig. 1b and envelop the laboratory data. A repeat experiment by Wright and Petters (2013) should
310 result in a f_{ufz} curve falling within the percentile bounds 95 % of the time when considering only stochastic uncertainty.

To further evaluate the validity of the simulations, the parameters used are compared with experimental conditions given in Wright and Petters (2013). IsoWR uses $N_{\text{tot}} = 1000$ which agrees with the reported range of 300–1500. The next parameter in question is $\sigma_g = 9.5$, which can be in-
315 terpreted as a systematic standard error in ISA due to the experimental methods of generating or dispensing droplets containing ATD acting as IN. We note this is different from an absolute ISA measurement error. Wright and Petters (2013) emulsified a mixture of oil and a bulk solution of water and ATD particles to form droplets with diameters of 50–250 μm . The variability in ISA should scale directly with the variability in droplet volumes (over 2 orders of magnitude), the variability
320 in ATD particle numbers, and the variability in ATD particle size. While not directly defined by Wright and Petters (2013), we are confident that the overall range in ISA should be well over 2 orders of magnitude and therefore, $\sigma_g = 9.5$ is a reasonable value for the lognormal distribution width parameter employed in the simulations in Fig. 1b to reproduce the experimental data. The third parameter in question is $A_g = 6.4 \times 10^{-3} \text{ cm}^2$. Unfortunately, an average ISA was not reported
325 by Wright and Petters (2013), but can be estimated using literature values of specific surface area (SSA) applying the Brunauer, Emmett and Teller gas adsorption method (Brunauer et al., 1938). It is important to note that surface area measurements are not unambiguous due to the fact that heterogeneous ice nucleation may involve layers of water molecules interacting with surface molecules (Cox et al., 2013). The BET technique is one of many in which particle surface area is measured,
330 and can be used to represent molecular available surface area. Bedjanian et al. (2013) report SSA for ATD used in Wright and Petters (2013) as $85 \pm 10 \text{ m}^2 \text{ g}^{-1}$. The ISA per drop can then be estimated from the drop volume, V_{drop} , and the density of water, ρ_w , using the equation $V_{\text{drop}} \cdot \rho_w \cdot \text{wt \%} \cdot \text{SSA}$. Considering only the variability in V_{drop} , average ISA per drop should range between 5.5×10^{-4} and $7.0 \times 10^{-2} \text{ cm}^2$. The A_g parameter in model simulation IsoWR falls within this range. Finally, J_{het}

335 for ATD in water droplets was investigated by Pinti et al. (2012) who reanalyzed ATD immersion
freezing data by Marcolli et al. (2007) but did not report J_{het} values. However, estimates can be made
following Knopf and Alpert (2013) accounting for $f_{\text{frz}} = 0.01$ and a nucleation time assumed to be
1 s, which yields J_{het} ranging from 5×10^6 to $1 \times 10^2 \text{ cm}^{-2} \text{ s}^{-1}$ between $T = 247.4$ and 252.8 K , in
reasonable agreement with $J_{\text{het}} = 2.6 \times 10^3 \text{ cm}^{-2} \text{ s}^{-1}$ used in IsoWR at 251 K .

340 The new model simulation presented here based entirely on CNT can describe freezing experi-
ments by Wright and Petters (2013) accounting for long nucleation time scales and a large number
of droplets considering variability in ISA. In addition, all crucial parameters applied are experimen-
tally supported, in particular J_{het} which is in agreement with independent studies (Marcolli et al.,
2007; Pinti et al., 2012). Therefore, the isothermal immersion freezing data set of Wright and Petters
345 (2013) can be entirely explained by a time and ISA dependent stochastic freezing process, in which
each droplet contains variable ISA. Droplet to droplet variability in ice nucleation efficiency is typ-
ically parameterized with a variable efficiency of sites to nucleate ice or different contact angles
(e.g. Niedermeier et al., 2011; Broadley et al., 2012). Droplet to droplet variability parameterized in
these ways and employing identical ISA can result in a deviation of f_{ufz} from a log-linear relation-
350 ship, similar to what is seen in Fig. 1. However, using a known ISA variability (Broadley et al., 2012;
Wright and Petters, 2013), we reveal that the observed deviation from a log-linear relationship can
be accounted for entirely by the ISA distribution. This implies that the droplet to droplet variability
in ice nucleation efficiency parameterized by a contact angle or active site distribution is potentially
unimportant.

355 Figure 2 shows results of isothermal freezing experiments by Broadley et al. (2012) for illite com-
pared to model simulation IsoBr and experimental results by Herbert et al. (2014) for the IN types
kaolinite and feldspar compared to model simulations IsoHE1 and IsoHE2, respectively (see Ta-
ble 1). The experimental data and \bar{f}_{ufz} for all model simulations are in agreement and fall within the
percentile bounds. Notice that the scatter in the isothermal immersion freezing data points is much
360 larger than for Wright and Petters (2013) shown in Fig. 1b. As previously discussed, this is entirely
due to a smaller number of droplets used in the laboratory experiments by Broadley et al. (2012)
($N_{\text{tot}} = 63$) and Herbert et al. (2014) ($N_{\text{tot}} = 40$) and thus, can be entirely attributed to the stochastic
nature of immersion freezing as expected by CNT. The model simulations capture this effect by pro-
ducing a wide range in f_{ufz} . Only one experiment was performed for each of the laboratory data sets
365 presented in Fig. 2 and if these experiments were repeated, f_{ufz} values would very likely not be the
same and may even exhibit a more linear or curved behavior with time. Repetition of experiments
should provide better estimates of \bar{f}_{ufz} and σ_{g} , but for any single experiment, f_{ufz} would still fall
within the given percentile bounds. In other words, additional experiments would better define the
mean of f_{ufz} and the uncertainty in the mean of f_{ufz} , but will not decrease the uncertainty bounds.
370 Only by using more droplets, e.g. Wright and Petters (2013), would a single experiment be more
statistically significant.

Parameters A_g and N_{tot} used in IsoBR are directly provided and used (Broadley et al., 2012). Droplet volumes in the experiment by Broadley et al. (2012) (Fig. 2a) varied by an order of magnitude. Considering the additional variability in particle numbers and size, total ISA variability should be larger than 1 order of magnitude. For IsoBR, $\sigma_g = 8.3$, in agreement with experimental conditions. J_{het} derived at $T = 243.3\text{K}$ by ABIFM is $1.25 \times 10^3 \text{cm}^{-2} \text{s}^{-1}$ and is in excellent agreement with model derived J_{het} at the same experimentally investigated T . Similar to Wright and Petters (2013), the deviation of f_{ufz} from a log-linear relationship can be completely accounted for by the experimentally constrained ISA distribution. Thus, laboratory derived isothermal immersion freezing of illite is entirely explained by CNT accounting for the stochastic nature of immersion freezing and variability in ISA.

The model simulation IsoHe1 shown in Fig. 2b uses the parameter $A_g = 1.2 \text{cm}^2$, in good agreement with experimentally derived $A_g = 2.4 \text{cm}^2$, for kaolinite using $\text{SSA} = 11.8 \text{m}^2 \text{g}^{-1}$ (Murray et al., 2011), 1.0 wt % concentration and $V_{\text{drop}} = 1 \mu\text{L}$. Herbert et al. (2014) did not report sufficient information to estimate an overall variability in ISA, therefore, comparison of σ_g to experimental conditions is difficult. As previously discussed, a repeat experiment may result in f_{ufz} exhibiting more linear or non-linear behavior with t within the calculated percentile bounds, i.e. within the stochastic uncertainty. Fig. 1A shows that a more linear or non-linear relationship of f_{ufz} with t implies a smaller or larger value of σ_g . Herbert et al. (2014) assumed that each droplet possessed the same ISA, however, this assumption is not supported due to the large stochastic uncertainty from the small number of applied droplets. In order to better assess σ_g , more experiments or employing a larger number of droplets are needed to obtain more accurate \bar{f}_{ufz} values. The ABIFM yields $J_{\text{het}} = 1.75 \times 10^{-2} \text{cm}^{-2} \text{s}^{-1}$ at $T = 255.15\text{K}$ and $a_w = 1.0$ which is within an order of magnitude of J_{het} used in IsoHE1. The agreement between simulated and experimental parameters implies that CNT can explain observed immersion freezing of kaolinite when variable ISA and stochastic uncertainty is considered.

Immersion freezing data of Herbert et al. (2014) for feldspar is reproduced by the model simulation IsoHE2. The parameters for IsoHE2 are given in Table 1. Average ISA for the data in Fig. 2 is $1.85 \times 10^{-2} \text{cm}^2$, similar to $A_g = 2.0 \times 10^{-2} \text{cm}^2$ used in IsoHE1. Droplets used in Herbert et al. (2014) were dispensed with a digital micropipet with high accuracy, thus it can be expected that the contribution of droplet volume variability to the σ_g parameter is low. However, large uncertainty in f_{ufz} limits a reliable experimental estimate of σ_g for comparison with model derived σ_g . To better constrain σ_g , more stochastic certainty is required by application of more droplets or conducting multiple experiments. Values of J_{het} for feldspar independent from Herbert et al. (2014) in the same temperature range to our knowledge do not exist making comparison difficult.

Model simulations IsoDI1-3 of isothermal immersion freezing experiments by Diehl et al. (2014) for illite acting as IN in wind tunnel levitation experiments are shown in Fig. 3. Simulation parameters are given in Table 1. Only one droplet was observed in each experiment, and approximately

45 experiments were conducted for each of the 3 data sets shown in Fig. 3. This is equivalent to
 410 1 experiment with $N_{\text{tot}} = 45$ droplets, since droplet freezing is independent of the freezing of other
 droplets. Excellent agreement is observed between simulated and experimental f_{ufz} . At $T = -18$ and
 -21°C , the ABIFM yields $J_{\text{het}} = 1.8 \times 10^{-2}$ and $2.6 \times 10^{-1} \text{ cm}^{-2} \text{ s}^{-1}$, respectively, and is in ex-
 cellent agreement with derived values in IsoDI1-3. It can be expected that σ_g is the same for all three
 415 simulations, due to the fact that Diehl et al. (2014) likely used identical bulk water-illite solution
 stock. However, the large uncertainties do not allow for an adequate constraint of σ_g . Nevertheless, a
 time dependent and stochastic immersion freezing process can reconcile observations when variable
 ISA is considered.

Depending on ISA variability, trajectories of model derived f_{ufz} over time are significantly al-
 tered and thus assuming identical ISA is not valid. It is well known that immersion freezing depends
 420 on surface area, i.e. an increase in ISA translates to an increase in nucleation rate. However, we
 note that variability in both t and ISA equally affect calculations of droplet freezing probabilities
 (Eq. 4) used in model simulations, and therefore neglecting time dependence will cause erroneous
 interpretation of immersion freezing data to the same degree as if the surface area dependence is ne-
 glected. This simple stochastic immersion freezing model accounting for ISA variability can explain
 425 the isothermal ice nucleation data of various experiments without invoking empirical parameteri-
 zations, assumptions of particle surface composition, and/or other modifications in parameters and
 interpretations.

3.2 Cooling rate model simulations of individual droplet freezing experiments

Cooling rate IFSs were performed to investigate the effects of variable ISA and N_{tot} on experimen-
 430 tally derived J_{het} and f_{frz} as a function of T . For a single cooling rate IFS, variable ISA per droplet
 is applied and used to calculate $P_{j,\text{frz}}$ from Eq. (10), and then Eq. (5) simulates freezing. Discrete
 δT steps are used in cooling IFSs and thus, this process is repeated for all droplets which remained
 unfrozen at each consecutive δT . The IFS stops after some T or when all droplets freeze, and the
 simulated freezing record is kept detailing which droplets froze or remained liquid at each T and
 435 their corresponding ISA. This is analogous to running an immersion freezing experiment in a labo-
 ratory setting and recording the observed number of frozen droplets or ice crystals as a function of
 T .

The simulated freezing record is treated as a freezing data set from which the assumption of iden-
 tical ISA can be tested. This is accomplished by re-calculating J_{het} from the simulated data. These
 440 (re-)calculations use n_{frz} , the length of the time interval, $\delta t = \delta T/r$, and either of two different ap-
 proaches in determining A_{tot} . For the first approach, A_g is assumed to be identical for all droplets,
 i.e. without the knowledge that immersion freezing was simulated for droplets with variable ISA
 in the first place. This is equal to assuming a monodisperse IN population in laboratory immer-
 sion freezing experiments resulting in an ‘‘apparent’’ heterogeneous ice nucleation rate coefficient,

445 $J_{\text{het}}^{\text{apparent}}(T)$, calculated by

$$J_{\text{het}}^{\text{apparent}}(T) = \frac{n_{\text{frz}}(T)}{n_{\text{ufz}}(T)A_g \frac{\delta T}{r}}, \quad (11)$$

where $n_{\text{ufz}}(T)$ is the number of unfrozen droplets at T and $A_{\text{tot}} = n_{\text{ufz}}A_g$. The second approach accounts for the variable ISA present in droplets resulting in the “actual” heterogeneous ice nucleation rate coefficient, $J_{\text{het}}^{\text{actual}}(T)$, calculated by

450
$$J_{\text{het}}^{\text{actual}}(T) = \frac{n_{\text{frz}}(T)}{\sum A_j \frac{\delta T}{r}}, \quad (12)$$

and $A_{\text{tot}} = \sum A_j$ is the total surface area contribution from droplets that remain liquid. Comparing results from Eqs. (11) and (12) allows evaluation of the assumption that all droplets have the same ISA, when they actually do not. In this way a null hypothesis is considered, that is if $J_{\text{het}}^{\text{apparent}}(T)$ and $J_{\text{het}}^{\text{actual}}(T)$ are the same, then the assumption of identical ISA is valid.

455 Poisson statistics are used to derive upper and lower fiducial limits of $J_{\text{het}}^{\text{apparent}}(T)$ and $J_{\text{het}}^{\text{actual}}(T)$ at $x = 0.999$ confidence for n_{frz} following Koop et al. (1997). The upper fiducial limit of the heterogeneous ice nucleation rate coefficient, $J_{\text{het}}^{\text{up}}$, accounts for additional freezing events occurring with a probability of x , than observed n_{frz} . Likewise, a lower fiducial limit of the heterogeneous ice nucleation rate coefficient, $J_{\text{het}}^{\text{low}}$, accounts for less than the observed n_{frz} occurring with a probability
460 of x . We refer to the upper and lower limits of n_{frz} as $n_{\text{frz}}^{\text{up}}$ and $n_{\text{frz}}^{\text{low}}$, respectively (Koop et al., 1997). The fiducial limits of $J_{\text{het}}^{\text{apparent}}$ and $J_{\text{het}}^{\text{actual}}$ for a single simulation can be calculated using Eqs. (11) and (12), but replacing n_{frz} with $n_{\text{frz}}^{\text{up}}$ or $n_{\text{frz}}^{\text{low}}$, respectively. Each simulation results in different $J_{\text{het}}^{\text{apparent}}$ and $J_{\text{het}}^{\text{actual}}$ values and different fiducial limits at the same T due to random sampling, therefore, averages are reported.

465 Figure 4 shows the results of two model simulations, Cr1 and Cr2, having $r = 0.5$ and 5.0 K min^{-1} , respectively. For all 10^5 IFSS, $\bar{J}_{\text{het}}^{\text{apparent}}$ and $\bar{J}_{\text{het}}^{\text{actual}}$ are shown in Fig. 4a and b as dashed lines, respectively, along with corresponding f_{frz} curves displayed in Fig. 4c and d. The parameterization of $J_{\text{het}}(T)$ for illite dust (Knopf and Alpert, 2013) with $m = 54.5$ and $c = -10.7$ used in Eq. (10) for each simulation is shown as the red line in Fig. 4a and b and referred to as the model input J_{het} .
470 Simulation parameters for Cr1 and Cr2 are given in Table 2.

According to CNT, two immersion freezing cooling rate experiments conducted at different r should result in identical J_{het} values due to the fact that J_{het} is independent of r . CNT is violated if significantly different J_{het} values are derived at different r . Figure 4a shows that values of $\bar{J}_{\text{het}}^{\text{apparent}}$ are not the same for model simulations Cr1 and Cr2. Also $\bar{J}_{\text{het}}^{\text{apparent}}$ is overestimated at higher freezing
475 ing temperatures and underestimated at lower freezing temperatures compared with model input $J_{\text{het}}(T)$. These significant differences do not support the null hypothesis and imply that when experimentally deriving J_{het} , the assumption that ISA per droplet is identical is invalid. Figure 4b shows that accounting for variable ISA, $\bar{J}_{\text{het}}^{\text{actual}}$ for Cr1 and Cr2 is consistent and in very good agreement with model input J_{het} (red curve) within the upper and lower fiducial limits. In addition, $\bar{J}_{\text{het}}^{\text{actual}}$ for

480 the two simulations Cr1 and Cr2 are identical at the same T . We conclude that when accounting for variable ISA, immersion freezing results applying different r and ISA are consistent as predicted by CNT.

Towards warmer ($T > 248$ K) and colder temperatures ($T < 238$ K), the difference in upper and lower fiducial limits derived in Cr1 and Cr2 are much greater than for the mid temperature range
 485 ($238 < T < 248$ K). In fact the smallest difference occurs at $\bar{f}_{\text{frz}} \simeq 0.5$. This is because calculations are statistically more significant at the median freezing where n_{frz} is largest. Fewer droplets freeze at the beginning and end of a cooling process resulting in a wide fiducial limit range reaching up to 4 orders of magnitude (Fig. 4a and b) in spite of a high number of dropets used ($N_{\text{tot}} = 1000$). The corresponding percentile bounds of f_{frz} shown in Fig. 4c and d do not reflect a considerable
 490 uncertainty compared to the upper and lower fiducial limits (Fig. 4a and b). It is important to note that f_{frz} are identical in Fig. 4c and d, because surface area is not used to derive f_{frz} . This analysis suggest that values and uncertainties of f_{frz} are not suited to derive J_{het} and any corresponding error.

Previous immersion freezing experiments by Herbert et al. (2014) are modeled in CrHE1 and CrHE2 where $r = 0.2$ and 2.0 K min^{-1} , respectively, for the case of feldspar acting as IN. The pa-
 495 rameters σ_g and A_g from the IsoHE2 simulation are used in CrHE1 and CrHE2. Since Herbert et al. (2014) assumed identical ISA, experimentally derived J_{het} can be directly compared with $J_{\text{het}}^{\text{apparent}}$ from cooling rate model simulations.

Figure 5 shows experimentally derived f_{frz} and $J_{\text{het}}^{\text{apparent}}$ from Herbert et al. (2014) compared to results of model simulations CrHE1 and CrHE2. Parameters $m = 122.83$ and $c = -12.98$ are used
 500 in Eq. (6) to reproduce frozen fraction data (Fig. 5a) within 5 and 95% bounds. The laboratory data falls within percentiles and fiducial limits of f_{frz} and $J_{\text{het}}^{\text{apparent}}$, respectively. The model simulations are robust since the same A_g and σ_g are used in both cooling rate and isothermal experiments. Figure 5b displays the good agreement between $J_{\text{het}}^{\text{apparent}}$, and experimental data. However, it also demonstrates that assuming uniform ISA causes an erroneous dependency of experimentally derived J_{het} on r .
 505 Figure 5c shows $\bar{J}_{\text{het}}^{\text{actual}}$ with upper and lower fiducial limits derived from CrHE1 and CrHE2. When accounting for variable ISA, $\bar{J}_{\text{het}}^{\text{actual}}$ are in excellent agreement with the ABIFM parameterization derived in this study for feldspar IN. Furthermore, $\bar{J}_{\text{het}}^{\text{actual}}$ calculated for different r are identical as predicted by CNT, a similar finding as in the model simulations Cr1 and Cr2 (Fig. 4b). Therefore, $J_{\text{het}}(T)$ used here can be considered a new $J_{\text{het}}(\Delta a_w)$ parameterization for feldspar valid for $0.078 <$
 510 $\Delta a_w < 0.120$.

The differences between $\bar{J}_{\text{het}}^{\text{apparent}}$ and $\bar{J}_{\text{het}}^{\text{actual}}$ shown in Figs. 4a, b and 5b, c are further discussed. After simulated freezing of droplets with variable ISA is complete, $J_{\text{het}}^{\text{apparent}}$ is calculated using the simulated droplet freezing record but, with the assumption that ISA is identical for all droplets equal to A_g . As previously discussed, this is analogous to observing droplet freezing in the laboratory and
 515 calculating J_{het} once the experiment is finished assuming identical ISA. The slope of $\bar{J}_{\text{het}}^{\text{apparent}}$ is less steep than for $\bar{J}_{\text{het}}^{\text{actual}}$ as a function of T . We note that surface area is inversely proportional to J_{het} .

In the temperature range in which freezing is simulated, droplets with ISA less than A_g will likely freeze at colder T compared to droplets with ISA greater than A_g , which will likely freeze at warmer T . However, assuming identical ISA equal to A_g for all droplets either overestimates or underestimates the actual ISA present in droplets that freeze at colder and warmer temperatures, respectively. Due to the inverse relationship between A_g and J_{het} , calculations of $\bar{J}_{\text{het}}^{\text{apparent}}$ from Eq. (11) will be underestimated and overestimated at colder and warmer temperatures, respectively. As a consequence, the slope of $\bar{J}_{\text{het}}^{\text{apparent}}$ is less steep compared to model input J_{het} (red curve) as demonstrated in Figs. 4a and 5b. Therefore, assuming identical ISA in each droplet not only results in erroneous J_{het} values (for various applied r), but also misrepresentation of the slope J_{het} vs. T . Furthermore, simulated and experimentally derived $J_{\text{het}}^{\text{apparent}}$ for $r = 0.2$ and 2.0 K min^{-1} (Fig. 5b) are different by about 1 order of magnitude at the same T . In separate model simulations not shown here, applying r different by 2 orders of magnitude yields $J_{\text{het}}^{\text{apparent}}$ values that differ by 2 orders of magnitude. This means that assuming identical ISA in each droplet implicitly imposes a cooling rate dependence on $J_{\text{het}}^{\text{apparent}}$.

Model simulations CrDI1 and CrDI2 of immersion freezing experiments by Diehl et al. (2014) for illite acting as IN probed in acoustic levitation experiments are shown in Fig. 6. Simulation parameters are given in Table 2. A non-linear r was used in Diehl et al. (2014) and was the same for both experiments and model simulations, but the ISA per droplet was varied. Diehl et al. (2014) reported an ISA per drop of 7.1×10^{-1} and $7.1 \times 10^{-3} \text{ cm}^2$ in the 2 different sets of experiments. When using these exact values in conjunction with the other parameters, model simulations cannot reproduce experimental f_{frz} . This is in spite of the excellent performance of IsoBr for reproducing droplet freezing initiated by illite IN from Broadley et al. (2012). In attempt to reconcile results from Diehl et al. (2014) with previous literature data (Broadley et al., 2012; Knopf and Alpert, 2013), model derived f_{frz} are fit to experimental f_{frz} yielding two different parameter values of $A_g = 2.94$ and $2.91 \times 10^{-2} \text{ cm}^2$ used in CrDI1 and CrDI2, respectively. We note that fitted A_g values differ only by a factor of 4 from values reported by (Diehl et al., 2014) and therefore, are in reasonable agreement. However, calculated $J_{\text{het}}^{\text{apparent}}$ values shown in Fig. 6b still use ISA of 7.1×10^{-1} and $7.1 \times 10^{-3} \text{ cm}^2$ as reported by Diehl et al. (2014).

Figure 6a shows that simulated and experimental f_{frz} are in agreement when accounting for ISA variability ($\sigma_g = 5.7$). Experimental values of $J_{\text{het}}^{\text{apparent}}$ displayed in Fig. 6b are in agreement with model derived $\bar{J}_{\text{het}}^{\text{apparent}}$. This result is robust since experimental $J_{\text{het}}^{\text{apparent}}$ data was not used in fitting f_{frz} . Accounting for the actual variability in ISA used to simulate freezing, $J_{\text{het}}^{\text{actual}}$ shown in Fig. 6c is in perfect agreement with the ABIFM parameterization for illite (Knopf and Alpert, 2013). Again, the data and model supports a stochastic, time dependent immersion freezing process to describe laboratory data considering variable ISA.

A major inconsistency in experimental and simulated $J_{\text{het}}^{\text{apparent}}$ shown in Fig. 6b is discussed for the case when different ISA are applied. According to CNT, J_{het} is independent of surface area. This

means that if two experiments are performed with different ISA but use the same r , J_{het} should be the same as a function of T . However, simulated and experimentally derived $\bar{J}_{\text{het}}^{\text{apparent}}(T)$ deviate by more than 1 order of magnitude. Clearly, $J_{\text{het}}^{\text{apparent}}$ values violate CNT, but this is the cause of assuming identical ISA. In fact, this freezing behavior also contradicts all surface-based empirical parameterization of immersion freezing, such as determining $n_s(T)$, or the number of active sites per particle surface area (Murray et al., 2012; Hoose and Möhler, 2012). This result could potentially impact immersion freezing experiments conducted as a function of ISA that assume identical ISA, thereby implicitly imposing a surface area dependence on $J_{\text{het}}^{\text{apparent}}$ or $n_s(T)$. Accounting for the experimental uncertainty and variability in ISA may reconcile experimental data.

3.3 Continuous flow and cloud chamber immersion freezing experiments

Model simulations IsoCFDC and IsoLACIS (see Table 1) reproduce experimental results of Wex et al. (2014) who used 2 ice nucleation instrumentation, (i) a continuous flow diffusion chamber (CFDC) (Rogers et al., 2001; DeMott et al., 2010) and (ii) the Leipzig aerosol cloud interaction simulator (LACIS) (Hartmann et al., 2011), respectively, to observe immersion freezing of 300 nm mobility diameter selected kaolinite particles as a function of T and $\text{RH} > 100\%$. It is important to note that for both instruments, droplet freezing is not observed and instead, the number of ice crystals is optically detected. Thus, f_{fz} is calculated from the ratio between observed ice crystal and aerosol numbers per volume of air. The model simulation parameter N_{tot} is derived from known experimental parameters, including residence time, $t_r = 5\text{ s}$, flow rate, $Q = 1.0\text{ L min}^{-1}$, and kaolinite particle concentrations, $N_p = 10\text{ cm}^{-3}$ (Wex et al., 2014). By defining a single IFS over an interval of time equal to t_r , $N_{\text{tot}} = N_p Q t_r = 833$ particles per IFS. Similarly for LACIS, $Q = 0.08\text{ L min}^{-1}$, $t_r = 1.6\text{ s}$, and $N_{\text{tot}} = 21$ particles per IFS. Note that minimum f_{fz} values for CFDC and LACIS presented in Wex et al. (2014) are approximately equal to $1/N_{\text{tot}}$. We run 1440 and 6000 isothermal IFSs for IsoCFDC and IsoLACIS, respectively, equivalent to 2 h averages as done in Wex et al. (2014). Simulation parameters for IsoCFDC and IsoLACIS are given in Table 1.

Figure 7 shows that simulated f_{fz} for IsoCFDC and IsoLACIS agree very well with CFDC and LACIS data by Wex et al. (2014). However, some data points fall outside of the 5 and 95 percentiles (Fig. 7a), which may imply that a greater uncertainty exists that cannot be explained by a stochastic freezing process. This may be due, in part, to uncertainty in ice crystal optical detection which is not accounted for in model simulations. The surface area for spherical 300 nm particles is $A_{300\text{nm}} = 2.8 \times 10^{-9}\text{ cm}^2$. However, the assumption that a kaolinite particle with an electrical mobility diameter of 300 nm is equal to a 300 nm diameter sphere is likely not true, due to shape irregularities, variable density, void fractions, multiple charges, and other geometries (DeCarlo et al., 2004; Slowik et al., 2004; Zelenyuk et al., 2006; Schmid et al., 2007; Park et al., 2008) with a tendency for greater surface area than assumed. Additionally, particles of larger diameter, and thus larger surface area, may have the same electrical mobility due to the presence of multiple charges. Therefore, a

590 distribution of particle surface area can be expected. Following Wiedensohler and Fissan (1988), the probability for particles having multiple charges as a function of particle diameter, $P(\ln D_p)$, at a constant electrical mobility diameter of 300nm is shown in Fig. S1. The distribution $P(\ln D_p)$ is a probability density function from which particle diameters are sampled in simulations IsoCFDC and IsoLACIS. Individual sampled particle surface area is calculated assuming spherical particles.

595 Calculations of $J_{\text{het}}^{\text{apparent}}$ and $J_{\text{het}}^{\text{actual}}$ assuming constant ISA equal to $A_{300\text{nm}}$ or accounting for variable ISA, respectively, in IsoCFDC and IsoLACIS are shown in Fig. 7b. We find agreement between $J_{\text{het}}^{\text{apparent}}$ and data by Wex et al. (2014) when accounting for multiple particle charges predicted by Wiedensohler and Fissan (1988). Furthermore, assuming that the electrical mobility diameter corresponds to the physical particle diameter and the particle being spherical in geometry does not
600 significantly overestimate ice nucleation kinetics within the uncertainty bounds which span 2-5 orders of magnitude. The model input J_{het} represents a new parameterization for Fluka kaolinite where $m = 31.32$ and $c = -2.07$ following the ABIFM applicable for $0.220 < \Delta a_w < 0.305$.

Wex et al. (2014) presented a detailed immersion freezing analysis of various kaolinite particle sizes and types of coatings, simulating all these cases is beyond the scope of this paper. However,
605 we are certain that model simulations which use the same $J_{\text{het}}(T, a_w)$ will hold for all IN systems at all T and RH based solely on the fact that the same physical and statistical principles apply. In other words, prediction of immersion freezing kinetics (i.e. using J_{het}) in the simulations is independent of experimentally applied ISA, particle size, and particle coating type (assuming the coating dissolves when water is taken up and does not react with the IN surface). These findings demonstrate that our
610 new model simulations and the ABIFM are applicable for ice nucleation studies using a CFDC as previously shown by Knopf and Alpert (2013) and additionally LACIS.

IFSs are used to describe AIDA chamber immersion freezing experiments applying natural dust IN by Niemand et al. (2012) in model simulations CrNI1 and CrNI2. Among the different types of natural dust investigated, we choose 2 Asian dust experiments at $-20.1 < T < -28.1^\circ\text{C}$ and
615 $-14.3 < T < -22.4^\circ\text{C}$ (see ACI04_19 and ACI04_16 in Tables 2 and 3 in Niemand et al., 2012). A continuous non-linear cooling rate with time due to adiabatic expansion is fitted to experimental trajectories using a 4th order polynomial function. In AIDA experiments water saturation is typically reached after cooling begins. To mimic this process, ice particle production in model simulations is allowed after 80 s of cooling (see Fig. 2 in Niemand et al., 2012). Ice crystal concentration in an
620 aerosol sampling flow of 5 L min^{-1} , from the chamber is observed every 5 s using an optical particle counter (Benz et al., 2005), thus a volume of 0.42L of air is simulated. Total particle numbers in the simulated volume are on the order of 10^5 which agree well with minimum reported f_{fritz} of about 10^{-5} . Niemand et al. (2012) reported lognormal surface-size distributions with parameters, $d_{S,\text{median}}$ and σ_g of polydisperse aerosol population. In CrNI1 and CrNI2, A_j is derived by sampling particle diameters from the corresponding number-size distributions and assuming spherical particles.
625 Sampling stops when A_{tot} equals total surface area reported by Niemand et al. (2012). As previously

discussed, assuming spherical particles results in a bias of $J_{\text{het}}(T)$, i.e. the slope of $J_{\text{het}}^{\text{apparent}}(T)$ is always underestimated (Fig. 4a). This assumption also underestimates total surface area resulting in erroneously high experimentally derived $J_{\text{het}}^{\text{actual}}(T)$ values compared with $J_{\text{het}}^{\text{actual}}(T)$ as demonstrated
630 in Fig. 7b. Experimentally derived J_{het} is not available and so the ABIFM parameters m and c are fitted to experimentally derived f_{frz} data. Model simulation parameters for CrNI1 and CrNI2 are given in Table 2.

Figure 8 shows simulated f_{frz} and $J_{\text{het}}^{\text{actual}}$ from CrNI1 and CrNI2 and the time evolution of simulated ice crystal concentration in CrNI1 observed during the experiments. Simulated f_{frz} (Fig. 8a)
635 fall within the experimental uncertainty reported by Niemand et al. (2012) and the scatter in the data for all dust types. Narrow 5 and 95 % bounds are attributable to large N_{tot} on the order of 10^5 droplets per cooling simulation. Ice particle concentrations over time in CrNI1 are shown (insert in Fig. 8a) and are in excellent agreement with observations. It is important to note that ice crystal concentration data was not used for fitting parameters m and c . Figure 8b shows $\bar{J}_{\text{het}}^{\text{actual}}$ and upper and lower fiducial limits.
640 As frozen fraction decreases the fiducial limits become broader ranging from 0.8 to 2.5 orders of magnitude. We conclude that our model simulations are suitable for describing laboratory immersion freezing in AIDA cloud chamber and further support the necessity of quantification of ISA variability in the derivation of ice nucleation kinetics.

Notice that in Fig. 8a, the vertical scatter in the experimental data increases at warmer T and for
645 low f_{frz} , which implies that uncertainty likely increases as f_{frz} decreases. Since aerosol numbers and surface area in the experiments by Niemand et al. (2012) are relatively the same for all experiments, decreasing f_{frz} implies fewer detected ice crystals or decreasing numbers of ice nucleation events resulting in an increase in experimental uncertainty. A deterministic (singular) approach for interpretation and analysis of ice crystal production, which inherently ignores stochastic freezing, cannot
650 explain the increase in the data scatter for smaller f_{frz} values at warmer T . These observations can be explained by a stochastic and time-dependent immersion freezing process. We note that other measurement uncertainties may exist which may not be captured either by a deterministic approach or by our model. However, we conclude that stochastic uncertainty is important to consider for future ice nucleation studies. The fiducial limits of $J_{\text{het}}^{\text{actual}}$ shown in Fig. 8b, in fact, capture this effect of
655 larger scatter as T increases implying the uncertainty in observed ice nucleation kinetics increases. Since the freezing efficiency of Asian dust was shown to be similar for Saharan, Canary Island, and Israeli dust (Niemand et al., 2012), the new ABIFM parameterization of $J_{\text{het}}(T, a_w)$ derived here is applicable for natural dust.

4 Simulation findings and uncertainty analysis

660 Our results strongly suggest that laboratory immersion freezing studies should provide accurate estimates of ISA variability in droplets. We find that simplified assumptions about ISA can result in

misinterpretation and miscalculation of J_{het} values. This includes assuming identical surface area, which implicitly imposes a dependence of J_{het} on both ISA and r . Future laboratory immersion freezing studies should also consider the stochastic nature of ice nucleation following CNT and resulting uncertainties. When only a single ice nucleation experiment is performed or too few droplets are used, stochastic uncertainty can potentially be very large and may limit data interpretation. Once again, stochastic uncertainty refers to large or small expected data scatter from observing small or large numbers of freezing events, respectively. The surface area based deterministic approach deriving $n_s(T)$ is an alternative to calculating J_{het} , but does not consider stochastic effects or effect of time in analysis of immersion freezing. By design, $n_s(T)$ should therefore, not have any dependence on r . However, this is not supported as $n_s(T)$ has been observed to be dependent on r for feldspar and kaolinite (Herbert et al., 2014).

The model simulation and laboratory data sets investigated here were performed for IN immersed in pure water droplets. However, aqueous solution droplets having $a_w < 1.0$ are frequently present in the atmosphere at supercooled temperatures and subsaturated conditions (i.e. RH < 100%). The ABIFM (Eqs. 6–8) inherently and accurately accounts for these conditions and thus, provides a complete description of immersion freezing for laboratory experiments, as well as cloud models under atmospherically relevant T and RH. We suggest that future isothermal and cooling rate dependent immersion freezing studies investigate aqueous solution droplets in addition to water droplets (e.g. Archuleta et al., 2005; Alpert et al., 2011b; Wex et al., 2014), providing additional data sets to constrain ice nucleation kinetics and to validate and expand ABIFM and other parameterizations.

Uncertainty analysis is crucial for the interpretation of laboratory immersion freezing results. Here we present a quantitative uncertainty analysis of J_{het} , by defining ΔJ_{het} as the total uncertainty derived from individual contributions of statistical uncertainty due to N_{tot} , temperature accuracy referred to as ΔT , a_w or RH accuracy referred to as ΔRH , ISA variability expressed as σ_g , and accuracy of measuring absolute surface area referred to as ΔA_g . This uncertainty analysis is applicable to both isothermal and cooling rate dependent immersion freezing experiments. It is convenient to quantify ΔJ_{het} in the form of a $\frac{\times}{\pm}$ error instead of a typical \pm error due to J_{het} varying exponentially over a linear range in T . If $J_{\text{het}} = 100 \text{ cm}^{-2} \text{ s}^{-1}$ with a factor of ± 3 error for example, then $\Delta J_{\text{het}} = \frac{\times}{\pm} 3$ equivalent to $J_{\text{het}} = 100 \frac{\times 3}{\pm 3} = 100 \frac{+200}{-67} \text{ cm}^{-2} \text{ s}^{-1}$. In the following analysis, ΔJ_{het} is quantified as $\frac{\times}{\pm}$, representing a factor error.

The uncertainty due to stochastic freezing is derived by running 10^5 IFSs with different values of N_{tot} and calculating ΔJ_{het} where the widths of the fiducial limits are smallest, i.e. at $f_{\text{irz}} \simeq 0.5$. Thus, ΔJ_{het} derived from N_{tot} yields the smallest error estimate possible or the limit of greatest experimental accuracy. Figure 9a illustrates that smaller N_{tot} results in larger ΔJ_{het} . When $N_{\text{tot}} = 30$ for example, $\Delta J_{\text{het}} = \frac{\times 15}{\pm 5}$, and when $N_{\text{tot}} = 1000$, $\Delta J_{\text{het}} = \frac{\times 1.3}{\pm 1.3}$. The uncertainty contribution due to ΔT is calculated using the slope of J_{het} vs. T following a similar procedure as in Riechers et al. (2013). Using the ABIFM at various temperature ranges and for different IN types (Knopf and Alpert, 2013),

J_{het} varies by a factor of 7.5 ± 5.5 per degree K. This means that if $\Delta T = \pm 1.0 \text{ K}$, $\Delta J_{\text{het}} = \times_{\div} 7.5$ on average, but can be $\times_{\div} 2$ or $\times_{\div} 13$ depending on the IN type and the range in T and RH. For example, $\Delta T = \pm 0.5 \text{ K}$ translates to $\Delta J_{\text{het}} = \times_{\div} 3.75$ as displayed in Fig. 9a. Considering the uncertainty in RH, Eq. (6) is used to derive $\Delta J_{\text{het}} = J_{\text{het}}(\Delta a_w) / J_{\text{het}}(\Delta a_w \pm \Delta \text{RH}) = 10^{m \Delta \text{RH}}$. Values of m in Eq. (6) are taken from this study and from Knopf and Alpert (2013) ranging from 15–123 and results in 69 on average. The mean and range of ΔJ_{het} due to ΔRH are shown in Fig. 9b. For example, if $\Delta \text{RH} = \pm 3\%$, then $\Delta J_{\text{het}} = \times_{\div} 117$ on average. If ISA per droplet varies in an experiment, but is assumed to be uniform, J_{het} is overestimated for $f_{\text{frz}} < 0.5$ and underestimated for $f_{\text{frz}} > 0.5$. This effect is quantified by allowing σ_g to vary and calculating the ratio $\Delta J_{\text{het}} = \bar{J}_{\text{het}}^{\text{apparent}} / \bar{J}_{\text{het}}^{\text{actual}}$ evaluated at $f_{\text{frz}} = 0.1$ and 0.9 . The resulting ΔJ_{het} is displayed in Fig. 9c as a function of σ_g . If $\sigma_g = 10$, for example, then $\Delta J_{\text{het}} = \times_{\div}^{4} 20$ at $f_{\text{frz}} = 0.1$ and 0.9 . Finally, ΔJ_{het} is directly proportional to ΔA_g shown in Fig. 9c, e.g. if $\Delta A_g = \times_{\div} 5$, then $\Delta J_{\text{het}} = \times_{\div} 5$.

Figure 9 demonstrates that each experimental parameter contributes to the uncertainty in J_{het} . The total uncertainty in J_{het} can then be estimated by summing the error contributions due to N_{tot} , T , RH, σ_g , and A_g , respectively. Figure 9 shows dotted lines serving as example values of experimental uncertainties and corresponding ΔJ_{het} . Applying $N_{\text{tot}} = 30$, $\Delta T = \pm 0.5 \text{ K}$, $\Delta \text{RH} = \pm 3\%$, $\sigma_g = 10$, and $\Delta A_g = \times_{\div} 5$, results in $\Delta J_{\text{het}} = \times_{\div}^{148} 154$. If laboratory immersion freezing studies were to be conducted under these conditions, then the range in experimentally derived J_{het} should be over 4 orders of magnitude. Notice that the uncertainty due to RH alone can potentially dominate the total uncertainty. We hope that Fig. 9 provides guidance in conducting future immersion freezing studies.

We test our analysis to reproduce experimentally derived uncertainty. In Knopf and Alpert (2013), all experimentally derived J_{het} fell within ± 2 orders of magnitude as a function of the a_w criterion (Eq. 7) and as a result, this range was adapted as a conservative uncertainty estimate for the ABIFM model. The root mean square error of over 18 000 droplet freezing events for 6 different IN types was experimentally derived independent from model simulations, as an alternative uncertainty estimate exhibiting values as high as ± 1.3 orders of magnitude. Experimental parameters of studies used in the formulation of the ABIFM for pure water and aqueous solution droplets (Alpert et al., 2011a, b; Knopf and Forrester, 2011; Rigg et al., 2013; Knopf and Alpert, 2013) were about $N_{\text{tot}} = 300$, $\Delta T = \pm 0.3 \text{ K}$, $\Delta \text{RH} = \pm 1\%$, $\sigma_g = 5$, and $\Delta A_g = \times_{\div} 5$. Applying the analysis displayed in Fig. 9 results in an uncertainty of $\Delta J_{\text{het}} = \times_{\div}^{16} 18$ (spanning about 2.5 orders of magnitude) for the ABIFM model. This estimate is in excellent agreement with independently derived root mean square errors of J_{het} (Knopf and Alpert, 2013) and demonstrates the accuracy of our uncertainty analysis.

Model simulations reproduced observations of immersion freezing due to the IN illite by Diehl et al. (2014) and Broadley et al. (2012). These experimental data were included in a recent intercomparison study of illite IN immersion freezing by Hiranuma et al. (2015). Using 17 different instruments, experimentally derived $n_s(T)$ values were observed to increase from 10^{-3} to 10^8 cm^{-2} when T decreased from 263 to 236 K, equivalent to a slope of 0.5 orders of magnitude per 1 K. The in-

struments used are grouped by common methods and include, (i) cold stage (Broadley et al., 2012; Bingemer et al., 2012; Schill and Tolbert, 2013; Wright and Petters, 2013; O’Sullivan et al., 2014; Budke and Koop, 2015), (ii) liquid aliquots (Hill et al., 2014), (iii) droplet levitation (Szakáll et al., 2009; Diehl et al., 2014; Hoffmann et al., 2013), (iv) cloud chamber (Möhler et al., 2003; Niemand et al., 2012; Tajiri et al., 2013) and (v) continuous flow (Bundke et al., 2008; Stetzer et al., 2008; Welti et al., 2009; Lüönd et al., 2010; Chou et al., 2011; Friedman et al., 2011; Hartmann et al., 2011; Kanji et al., 2013; Tobo et al., 2013; Wex et al., 2014). The scatter in the n_s is roughly 3 orders of magnitude, but depending on T , a n_s range of 2 and 4 orders of magnitude can envelop the data. However, the authors provided no quantitative uncertainty analysis to explain this scatter. Since experimental methods and data reproduced by presented model simulations are included in Hiranuma et al. (2015) for illite, we apply the quantitative uncertainty analysis presented in Fig. 9 to provide a potential explanation of the data scatter. Although, J_{het} and $n_s(T)$ are different quantities, the contribution to their uncertainties is the same for ΔT , ΔRH , σ_g , ΔA_g .

Experimental T uncertainty for all methods typically ranged from ± 0.2 to ± 1.0 K, and hence $\Delta T = \pm 0.5$ is chosen as a representative value. Considering the slope n_s vs. T , $\Delta T = \pm 0.5$ contributes a factor of ~ 2 uncertainty to $n_s(T)$, or $\Delta n_s = \frac{\times}{\div} 2$. The ISA distribution width parameter of simulated experiments (Tables 1 and 2) is averaged to represent $n_s(T)$ data, yielding a reasonable value of $\sigma_g = 7$, resulting in $\Delta n_s = \frac{\times 3}{\div 12}$. The ISA measurement error is considered to be $\Delta A_g = \frac{\times}{\div} 5$, thus $\Delta n_s = \frac{\times}{\div} 5$. Calculation of $n_s(T)$ is not stochastic by design, and thus any uncertainty contribution due to N_{tot} on $n_s(T)$ was previously not considered (Hiranuma et al., 2015). Additionally, the intercomparison analysis ignores differences in experimental time scales in $n_s(T)$ derivation. However, this study demonstrates that the stochastic uncertainty can explain most immersion freezing data and therefore, likely contributes to the range of data scatter in $n_s(T)$. Typically, N_{tot} is about 50 which serves as a reasonable representation yielding $\Delta n_s = \frac{\times 8}{\div 4}$, although N_{tot} can vary between 10 and more than 1000 depending on the experiment. Previous immersion freezing experiments for illite IN have shown that when r or residence time differ by 1 order of magnitude, freezing temperatures shift by about 0.75 K on average (Broadley et al., 2012; Welti et al., 2012; Knopf and Alpert, 2013). As discussed in Hiranuma et al. (2015), cooling rates and residence times in the different instruments varied over ± 2 orders of magnitude, or $\Delta t = \frac{\times}{\div} 100$, corresponding to $\Delta T = \pm 1.5$ K, and thus contributing to an error of ± 0.75 orders of magnitude or $\Delta n_s = \frac{\times}{\div} 6$. Accounting for all uncertainties and making use of Fig. 9 results in $\Delta n_s = \frac{\times(2+3+5+8+6)}{\div(2+12+5+4+6)}$ for a total uncertainty of $\Delta n_s = \frac{\times 24}{\div 29}$, or an uncertainty range of 2.8 orders of magnitude. The vast majority of data in Hiranuma et al. (2015) fall within this uncertainty and implies that variability in $n_s(T)$ can be attributed to experimental, time-dependent, and stochastic uncertainties. It is important to note that the uncertainty due to neglecting time, ISA variability and stochastic effect contributes more to Δn_s , than T and ISA measurement error. Hiranuma et al. (2015) hypothesized that experimental procedures of droplet or particle preparation, including particle generation, size selection, ice crystal detection, particle loss at instrument

sampling inlets, contamination, inhomogeneous temperature, and differences in surface cation concentration between wet dispersed or dry dispersed particles may be the cause in measured scatter in
775 $n_s(T)$ data. These effects are not considered in the uncertainty analysis presented here, but may also contribute.

5 Atmospheric implications

The model simulations presented here are used to investigate effects of variable ISA on atmospheric ice nucleation. Only immersion freezing is considered, however, mixed-phase and cirrus clouds can
780 undergo other cloud microphysical effects such as homogeneous ice nucleation, deposition ice nucleation, contact ice nucleation, ice multiplication, ice crystal growth, water vapour depletion due to the Bergeron–Wegener–Findeisen process, entrainment and mixing, and ice crystal sedimentation. Aerosol populations are highly diverse, but for demonstrative purposes we only use a single INP type. The purpose here is not to simulate any physically realistic cloud, but to investigate the
785 sensitivity of ice particle production on σ_g . In 2 model simulations MPC1 and MPC2, IN particle diameters, D_p , are either uniform or sampled from a lognormal distribution, respectively. Parameters are given in Table 2. Surface area is calculated assuming spherical particles. We apply illite particles as IN with $N_p = 100 \text{ cm}^{-3}$ (air). Mixed-phase cloud conditions are assumed in which one particle is immersed inside of one dilute cloud droplet with $a_w \sim 1.0$.

790 Figure 10 presents the results of MPC1 and MPC2 applying $N_{\text{tot}} = 10^7$ illite particles in 100 L of air with an updraft velocity, $w = 100 \text{ cm s}^{-1}$, as a function of T , t , and height, h , where the first ice nucleation event occurs at $t = 0$ and $h = 0$. Simulated f_{frz} curves are shown in Fig. 10a, in addition to J_{het} and the ice saturation ratio, S_{ice} , as a function of T . As T decreases and t increases, J_{het} , S_{ice} and f_{frz} increase. Corresponding ice crystal concentrations derived using MPC1 and MPC2 are
795 displayed in Fig. 10b as the number of ice crystals formed per volume of air. Although homogeneous ice nucleation of droplets is not considered in the model, the temperature range in which this process becomes important is shaded in gray.

Values of f_{frz} derived in MPC2 are larger than for MPC1 and extend over a wider range of T as shown in Fig. 10a. As a result, the onset of ice nucleation, which occurs at $f_{\text{frz}} = 10^{-7}$ (or 10^{-2} ice
800 crystals L^{-1}), is about 5 K warmer for MPC2 compared to MPC1 (Fig. 10a). Figure 10b shows ice crystal concentrations of 0.01 and 10 L^{-1} (air) at 251 and 258 K, respectively, produced by the simulations. Note that when employing a distribution width between $\sigma_g = 1$ and 5, ice crystal numbers and f_{frz} values should fall between the red and blue curves, respectively. Our calculations indicate that onset ice nucleation in mixed-phase clouds may be significantly influenced by a polydispersed
805 atmospheric aerosol population. It can be expected that atmospheric ice crystals are produced across a broad range of temperatures, even at $T \geq -15^\circ\text{C}$. Furthermore, this result underscores the im-

portance of determining coarse mode aerosol particle numbers and total particle surface areas to improve our predictive understanding of atmospheric ice formation (Knopf et al., 2014).

6 Summary and conclusions

810 Immersion freezing simulations based on a droplet resolved stochastic ice nucleation process applicable for various types of IN and experiments are presented here for both isothermal conditions and applying a cooling rate, r . The parameters in the IFSs are all physically defined and measurable, including heterogeneous ice nucleation rate coefficients, J_{het} , the number of droplets at the start of an experiment, N_{tot} , the ISA, A_g , and the variability of ISA, σ_g , which is assumed to be lognormally
 815 distributed due to employed IN particle preparation and droplet generation. Alternatively, individually measured ISA per droplets can be used. For IFSs in which a cooling rate, r , is applied, J_{het} as a function of T and aqueous solution water activity, a_w , can be calculated following the water activity based immersion freezing model (ABIFM) applicable for both pure water ($a_w = 1.0$) and aqueous solution ($a_w < 1.0$) droplets. These IFSs generate frozen and unfrozen droplet fraction data,
 820 f_{ufz} and f_{frz} , respectively, and using a Monte Carlo method in which 10^5 IFSs are performed under the same conditions, 5 and 95% bounds are derived as uncertainty estimates.

The sensitivity of f_{ufz} on σ_g and N_{tot} was tested using sets of isothermal IFSs, where a single set is referred to as a model simulation. Uniform ISA (i.e. $\sigma_g = 1$) resulted in f_{ufz} (on a logarithmic scale) being linear with t . When ISA varied lognormally with parameters $\mu = \ln(A_g)$ and $\sigma = \ln(\sigma_g)$,
 825 where $\sigma_g > 1$, $\ln(f_{\text{ufz}})$ vs. t exhibit non-linear behavior. When larger or smaller N_{tot} was used, f_{ufz} had a smaller and larger uncertainty, respectively, due to the statistical significance of observing more freezing events. Effects of σ_g and N_{tot} on f_{ufz} are independent and thus, can be quantified apart from each other. These results demonstrate that in laboratory immersion freezing experiments, variable ISA imposes changes in trajectories of f_{ufz} and f_{frz} over time, and that the number of investigated
 830 droplets significantly impacts experimental uncertainty.

Cooling rate model simulations were used to test the validity of assuming uniform ISA. This was accomplished by recalculating J_{het} after simulation of immersion freezing in two ways, either (i) assuming uniform ISA referred to as the “apparent” ice nucleation rate coefficient, $J_{\text{het}}^{\text{apparent}}$, or (ii) accounting for variable ISA referred to as the “actual” ice nucleation rate coefficient, $J_{\text{het}}^{\text{actual}}$.
 835 When different r were applied in simulations, values of $J_{\text{het}}^{\text{apparent}}$ were significantly different from each other. When comparing experiments with different ISA but identical r , $J_{\text{het}}^{\text{apparent}}(T)$ was again significantly different. For $f_{\text{frz}} < 0.5$ and $f_{\text{frz}} > 0.5$, $J_{\text{het}}^{\text{apparent}}$ was over and underestimated, respectively, compared to $J_{\text{het}}^{\text{actual}}$, yielding an erroneous slope of $J_{\text{het}}^{\text{apparent}}(T)$. These results demonstrate that the assumption of identical ISA implicitly imposes a cooling rate and surface area dependence on
 840 experimentally derived $J_{\text{het}}(T)$. However, derivation of $J_{\text{het}}^{\text{actual}}$ from model simulations accounting

for variable ISA were consistent for different r and ISA, supporting a stochastic immersion freezing description as predicted by CNT.

Model simulations in which variable ISA was considered reproduced laboratory experiments using Arizona test dust (ATD) (Wright and Petters, 2013), illite (Broadley et al., 2012; Diehl et al., 2014), kaolinite (Wex et al., 2014; Herbert et al., 2014), feldspar (Herbert et al., 2014), and natural dusts from Asia, Israel, the Sahara desert and Canary Islands (Niemand et al., 2012) acting as IN. Despite whether isothermal or linear and nonlinear cooling rates were applied, modeled and experimental f_{frz} and f_{ufz} were in agreement within the stochastic uncertainty. More importantly, experimentally derived $J_{\text{het}}(T)$ and simulated $J_{\text{het}}^{\text{apparent}}$ were in agreement, indicating an imposed bias solely due to the assumption of uniform ISA and not to physical processes governing ice nucleation. Despite this fact, model simulations can correct for this introduced bias yielding “actual” values, or $J_{\text{het}}^{\text{actual}}$, which resulted in consistent agreement between different studies and additionally new a_w based parameterizations of $J_{\text{het}}(\Delta a_w)$ for feldspar and natural dusts.

A quantitative uncertainty analysis of J_{het} was presented applicable for experimental studies in which the contribution due to (i) N_{tot} , (ii) temperature accuracy referred to as ΔT , (iii) a_w or RH accuracy referred to as ΔRH , (iv) σ_g , and (v) the accuracy of A_g referred to as ΔA_g , were individually quantified. The following points summarize these error sources and give recommendations for future experimental studies:

- Applying too few N_{tot} or performing only a single ice nucleation experiment in laboratory studies results in highly uncertain freezing results. Therefore, repetition of immersion freezing experiments or a statistically significant number of droplets must be applied. We recommend using at least 100 droplets and three independent freezing cycles in order to better quantify data scatter and average J_{het} , f_{frz} , and f_{ufz} values. This contributes to a range of 0.75 orders of magnitude in the uncertainty of experimentally derived J_{het} .
- For different IN types, the slope of J_{het} vs. T is not the same and thus, the uncertainty due to ΔT is IN type dependent, but can be as high as 1 order of magnitude per 1 K. We recommended that ΔT remain $< \pm 0.5 \text{ K}$ to achieve an acceptable uncertainty contribution, i.e. half an order of magnitude.
- The greatest source of error stems from RH, or ΔRH . Immersion freezing experiments for $\text{RH} < 100\%$ should aim for ΔRH to be as small as possible. Current and future immersion freezing experiments should be designed to carefully control RH and quantify its uncertainty.
- Droplets in laboratory immersion freezing experiments will not have identical ISA, but will vary from droplet to droplet (σ_g) around some ISA value (A_g). Variability in ISA and corresponding uncertainty should be quantified and accounted for when analyzing ice nucleation experiments.

- Surface area and nucleation time scales clearly affect immersion freezing data. Common assumptions of ISA and neglecting the impact of variable experimental time scales will lead to an incomplete experimental accuracy and uncertainty. Consideration of these effects is recommended to narrow the uncertainty in predicting ice crystal formation.

880 The influence of variable ISA on ice crystal production in an idealized cloud model was investigated using two IFSs having $\sigma_g = 1$ and 5 (i.e. monodisperse and polydisperse IN populations, respectively). Ice nucleation occurred over a broader range of time and temperature resulting in greater ice particle production for $\sigma_g = 5$. Ice crystal concentrations, N_{ice} , in the range of 0.01–100 L⁻¹ (air) consistently occurred at temperatures about 5K warmer when applying polydispersed
885 IN populations compared to IFSs of monodispersed IN. Likewise, at a constant T , N_{ice} were consistently greater by two orders of magnitude. We suggest that field measurements should determine and consider the entire aerosol size distribution as a source of IN for implementation of a stochastic, time-dependent ice nucleation process characterized by J_{het} , which is easily parameterized following the ABIFM.

890 Our findings concerning laboratory immersion freezing experiments emphasize the importance of setting constraints on the minimum number of droplets and experimental trials that need to be employed for improved characterization of ISA per droplet. The results presented here resolves commonly used assumptions that contribute to additional uncertainty in predicting immersion freezing data for model implementation. The simulations use ABIFM, shown to be valid for various INP
895 types. We demonstrate that the ABIFM can reproduce immersion freezing by mineral dust for many vastly different experimental designs and measurement methods. Laboratory derived J_{het} values can aid in testing existing ABIFM parameterizations and formulating new ones. Their application to a very simple stochastic freezing model based on a binomial distribution in accordance with classical nucleation theory, can reconcile immersion freezing data for various IN types and measurement
900 techniques when the applied IN surface areas are treated more realistically. These findings hopefully stimulate further discussion on the analytical procedure and interpretation of immersion freezing and its implementation in atmospheric cloud and climate models.

Acknowledgements. This research was supported by the U.S. Department of Energy, Office of Science (BER), under Award Number DE-SC0008613.

905 **References**

- Alpert, P. A., Knopf, D. A., and Aller, J. Y.: Ice nucleation from aqueous NaCl particles with and without marine diatoms, *Atmos. Chem. Phys.*, 11, 5539–5555, doi:10.5194/acp-11-5539-2011, 2011a.
- Alpert, P. A., Knopf, D. A., and Aller, J. Y.: Initiation of the ice phase by marine biogenic surfaces in supersaturated gas and supercooled aqueous phases, *Phys. Chem. Chem. Phys.*, 13, 19 882–19 894, 910 doi:10.1039/c1cp21844a, pubs.rsc.org/en/Content/ArticleLanding/2011/CP/c1cp21844a, 2011b.
- Archuleta, C. M., DeMott, P. J., and Kreidenweis, S. M.: Ice nucleation by surrogates for atmospheric mineral dust and mineral dust/sulfate particles at cirrus temperatures, *Atmos. Chem. Phys.*, 5, 2617–2634, doi:10.5194/acp-5-2617-2005, 2005.
- Augustin-Bauditz, S., Wex, H., Kanter, S., Ebert, M., Niedermeier, D., Stolz, F., Prager, A., and Stratmann, F.: 915 The immersion mode ice nucleation behavior of mineral dusts: A comparison of different pure and surface modified dusts, *Geophys. Res. Lett.*, 41, 7375–7382, doi:10.1002/2014GL061317, 2014.
- Baker, M. B.: Cloud microphysics and climate, *Science*, 276, 1072–1078, doi:10.1126/science.276.5315.1072, 1997.
- Bedjanian, Y., Romanias, M. N., and El Zein, A.: Uptake of HO₂ radicals on Arizona Test Dust, *Atmos. Chem. Phys.*, 13, 6461–6471, doi:10.5194/acp-13-6461-2013, 2013. 920
- Benz, S., Megahed, K., Möhler, O., Saathoff, H., Wagner, R., and Schurath, U.: T-dependent rate measurements of homogeneous ice nucleation in cloud droplets using a large atmospheric simulation chamber, *J. Photochem. Photobiol. A*, 176, 208–217, doi:10.1016/j.jphotochem.2005.08.026, 2005.
- Bingemer, H., Klein, H., Ebert, M., Haunold, W., Bundke, U., Herrmann, T., Kandler, K., Müller-Ebert, 925 D., Weinbruch, S., Judt, A., Wéber, A., Nillius, B., Ardon-Dryer, K., Levin, Z., and Curtius, J.: Atmospheric ice nuclei in the Eyjafjallajökull volcanic ash plume, *Atmos. Chem. Phys.*, 12, 857–867, doi:10.5194/acp-12-857-2012, 2012.
- Boucher, O., Randall, D., Artaxo, P., Bretherton, C., Feingold, G., Forster, P., Kerminen, V.-M., Kondo, Y., Liao, H., Lohmann, U., Rasch, P., Satheesh, S. K., Sherwood, S., B., S., and Y., Z. X.: Climate Change 930 2013: The Physical Science Basis. Contribution of Working Group I to the Fifth Assessment Report of the Intergovernmental Panel on Climate Change, chap. 8. Clouds and Aerosols, pp. 571–657, Cambridge University Press, Cambridge, United Kingdom and New York, NY, USA, 2013.
- Broadley, S. L., Murray, B. J., Herbert, R. J., Atkinson, J. D., Dobbie, S., Malkin, T. L., Condliffe, E., and Neve, L.: Immersion mode heterogeneous ice nucleation by an illite rich powder representative of atmospheric mineral dust, *Atmos. Chem. Phys.*, 12, 287–307, doi:10.5194/acp-12-287-2012, 935 www.atmos-chem-phys.net/12/287/2012/, 2012.
- Brunauer, S., Emmett, P. H., and Teller, E.: Adsorption of gases in multimolecular layers, *J. Am. Chem. Soc.*, 60, 309–319, doi:10.1021/ja01269a023, 1938.
- Budke, C. and Koop, T.: BINARY: an optical freezing array for assessing temperature and time dependence of 940 heterogeneous ice nucleation, *Atmos. Meas. Tech.*, 8, 689–703, doi:10.5194/amt-8-689-2015, 2015.
- Bundke, U., Nillius, B., Jaenicke, R., Wetter, T., Klein, H., and Bingemer, H.: The fast ice nucleus chamber, FINCH, *Atmos. Res.*, 90, 180–186, doi:10.1016/j.atmosres.2008.02.008, 2008.
- Chen, T., Rossow, W. B., and Zhang, Y. C.: Radiative effects of cloud-type variations, *Tellus A*, 50, 259–264, doi:10.1175/1520-0442(2000)013<0264:REOCTV>2.0.CO;2, 2000.

- 945 Chou, C., Stetzer, O., Weingartner, E., Jurányi, Z., Kanji, Z. A., and Lohmann, U.: Ice nuclei properties within a Saharan dust event at the Jungfraujoch in the Swiss Alps, *Atmos. Chem. Phys.*, 11, 4725–4738, doi:10.5194/acp-11-4725-2011, 2011.
- Connolly, P. J., Möhler, O., Field, P. R., Saathoff, H., Burgess, R., Choulaton, T., and Gallagher, M.: Studies of heterogeneous freezing by three different desert dust samples, *Atmos. Chem. Phys.*, 9, 2805–2824, doi:10.5194/acp-9-2805-2009, 2009.
- 950 Cox, S. J., Raza, Z., Kathmann, S. M., Slatara, B., and Michaelides, A.: The microscopic features of heterogeneous ice nucleation may affect the macroscopic morphology of atmospheric ice crystals, *Faraday Discuss.*, 167, 389–403, doi:10.1039/c3fd00059a, 2013.
- DeCarlo, P. F., Slowik, J. G., Worsnop, D. R., Davidovits, P., and Jimenez, J. L.: Particle morphology and density characterization by combined mobility and aerodynamic diameter measurements. Part 1: Theory, *Aerosol Sci. Technol.*, 38, 1185–1205, doi:10.1080/027868290903907, 2004.
- 955 DeMott, P. J., Prenni, A. J., Liu, X., Kreidenweis, S. M., Petters, M. D., Twohy, C. H., Richardson, M. S., Eidhammer, T., and Rogers, D. C.: Predicting global atmospheric ice nuclei distributions and their impacts on climate, *P. Natl. A. Sci.*, 107, 11 217–11 222, doi:10.1073/pnas.0910818107, 2010.
- 960 Diehl, K., Debortshäuser, M., Eppers, O., Schmithüsen, H., Mitra, S. K., and Borrmann, S.: Particle surface area dependence of mineral dust in immersion freezing mode: investigations with freely suspended drops in an acoustic levitator and a vertical wind tunnel, *Atmos. Chem. Phys.*, 14, 12 343–12 355, doi:10.5194/acp-14-12343-2014, 2014.
- Friedman, B., Kulkarni, G., Beránek, J., Zelenyuk, A., Thornton, J. A., and Cziczo, D. J.: Ice nucleation and droplet formation by bare and coated soot particles, *J. Geophys. Res.*, 116, D17 203, doi:10.1029/2011JD015999, 2011.
- 965 Haag, W., Kärcher, B., Ström, J., Minikin, A., Lohmann, U., Ovarlez, J., and Stöhl, A.: Freezing thresholds and cirrus cloud formation mechanisms inferred from in situ measurements of relative humidity, *Atmos. Chem. Phys.*, 3, 1791–1806, doi:10.5194/acp-3-1791-2003, 2003.
- 970 Hartmann, S., Niedermeier, D., Voigtländer, J., Clauss, T., Shaw, R. A., Wex, H., Kiselev, A., and Stratmann, F.: Homogeneous and heterogeneous ice nucleation at LACIS: operating principle and theoretical studies, *Atmos. Chem. Phys.*, 11, 1753–1767, doi:10.5194/acp-11-1753-2011, 2011.
- Hegg, D. A. and Baker, M. B.: Nucleation in the atmosphere, *Rep. Prog. Phys.*, 72, 056 801, doi:10.1088/0034-4885/72/5/056801, 2009.
- 975 Herbert, R. J., Murray, B. J., Whale, T. F., Dobbie, S. J., and Atkinson, J. D.: Representing time-dependent freezing behaviour in immersion mode ice nucleation, *Atmos. Chem. Phys.*, 14, 8501–8520, doi:10.5194/acp-14-8501-2014, 2014.
- Hill, T. C. J., Moffett, B. F., DeMott, P. J., Georgakopoulos, D. G., Stumpa, W. L., and Franca, G. D.: Measurement of ice nucleation-active bacteria on plants and in precipitation by quantitative PCR, *Appl. Environ. Microbiol.*, 80, 1256–1267, doi:10.1128/AEM.02967-13, 2014.
- 980 Hiranuma, N., Augustin-Bauditz, S., Bingemer, H., Budke, C., Curtius, J., Danielczok, A., Diehl, K., Dreischmeier, K., Ebert, M., Frank, F., Hoffmann, N., Kandler, K., Kiselev, A., Koop, T., Leisner, T., Möhler, O., Nillius, B., Peckhaus, A., Rose, D., Weinbruch, S., Wex, H., Boose, Y., DeMott, P. J., Hader, J. D., Hill, T. C. J., Kanji, Z. A., Kulkarni, G., Levin, E. J. T., McCluskey, C. S., Murakami, M., Murray, B. J., Niedermeier,

- 985 D., Petters, M. D., O'Sullivan, D., Saito, A., Schill, G. P., Tajiri, T., Tolbert, M. A., Welti, A., Whale, T. F.,
Wright, T. P., and Yamashita, K.: A comprehensive laboratory study on the immersion freezing behavior of
illite NX particles: a comparison of 17 ice nucleation measurement techniques, *Atmos. Chem. Phys.*, 15,
2489–2518, doi:10.5194/acp-15-2489-2015, 2015.
- Hoffmann, N., Duft, D., Kiselev, A., and Leisner, T.: Contact freezing efficiency of mineral dust aerosols stud-
990 ied in an electrodynamic balance: quantitative size and temperature dependence for illite particles, *Faraday
Discuss.*, 165, 383–390, doi:10.1039/C3FD00033H, 2013.
- Hoose, C. and Möhler, O.: Heterogeneous ice nucleation on atmospheric aerosols: a review of results from
laboratory experiments, *Atmos. Chem. Phys.*, 12, 9817–9854, doi:10.5194/acp-12-9817-2012, 2012.
- Iannone, R., Chernoff, D. I., Pringle, A., Martin, S. T., and Bertram, A. K.: The ice nucleation ability of one
995 of the most abundant types of fungal spores found in the atmosphere, *Atmos. Chem. Phys.*, 11, 1191–1201,
doi:10.5194/acp-11-1191-2011, <http://www.atmos-chem-phys.net/11/1191/2011/>, 2011.
- Kanji, Z. A., Welti, A., Chou, C., Stetzer, O., and Lohmann, U.: Laboratory studies of immersion and de-
position mode ice nucleation of ozone aged mineral dust particles, *Atmos. Chem. Phys.*, 13, 9097–9118,
doi:10.5194/acp-13-9097-2013, 2013.
- 1000 Knopf, D. A. and Alpert, P. A.: A water activity based model of heterogeneous ice nucleation kinetics for
freezing of water and aqueous solution droplets, *Farad. Discuss.*, 165, 513–534, doi:10.1039/c3fd00035d,
2013.
- Knopf, D. A. and Forrester, S.: Freezing of water and aqueous NaCl droplets coated by organic mono-
layers as a function of surfactant properties and water activity, *J. Phys. Chem. A*, 115, 5579–5591,
1005 doi:10.1021/jp2014644, 2011.
- Knopf, D. A., Alpert, P. A., Wang, B., O'Brien, R. E., Kelly, S. T., Laskin, A., Gilles, M. K., and Moffet, R. C.:
Microspectroscopic imaging and characterization of individually identified ice nucleating particles from a
case field study, *J. Geophys. Res.*, 119, 10 365–10 381, doi:10.1002/2014JD021866, 2014.
- Koop, T. and Zobrist, B.: Parameterizations for ice nucleation in biological and atmospheric systems, *Phys.*
1010 *Chem. Chem. Phys.*, 11, 10 839–10 850, doi:10.1039/B914289D, 2009.
- Koop, T., Luo, B. P., Biermann, U. M., Crutzen, P. J., and Peter, T.: Freezing of HNO₃/H₂SO₄/H₂O solutions
at stratospheric temperatures: Nucleation statistics and experiments, *J. Phys. Chem. A*, 101, 1117–1133,
doi:10.1021/jp9626531, 1997.
- Koop, T., Luo, B. P., Tsias, A., and Peter, T.: Water activity as the determinant for homogeneous ice nucleation
1015 in aqueous solutions, *Nature*, 406, 611–614, doi:10.1038/35020537, 2000.
- Kulkarni, G., Fan, J., Comstock, J. M., Liu, X., and Ovchinnikov, M.: Laboratory measurements and
model sensitivity studies of dust deposition ice nucleation, *Atmos. Chem. Phys.*, 12, 7295–7308,
doi:10.5194/acp-12-7295-2012, 2012.
- Liu, X., Penner, J. E., J., G. S., and Wang, M.: Inclusion of ice microphysics in the NCAR community atmo-
1020 spheric model version 3 (CAM3), *J. Climate*, 20, 4526–4547, doi:10.1175/JCLI4264.1, 2007.
- Lohmann, U. and Hoose, C.: Sensitivity studies of different aerosol indirect effects in mixed-phase clouds,
Atmos. Chem. Phys., 9, 8917–8934, doi:10.5194/acp-9-8917-2009, 2009.

- Lüönd, F., Stetzer, O., Welti, A., and Lohmann, U.: Experimental study on the ice nucleation ability of size-selected kaolinite particles in the immersion mode, *J. Geophys. Res.*, 115, D14 201, doi:10.1029/2009JD012959, 2010.
- 1025
- Marcolli, C., Gedamke, S., Peter, T., and Zobrist, B.: Efficiency of immersion mode ice nucleation on surrogates of mineral dust, *Atmos. Chem. Phys.*, 7, 5081–5091, doi:10.5194/acp-7-5081-2007, 2007.
- Möhler, O., Stetzer, O., Schaefers, S., Linke, C., Schnaiter, M., Tiede, R., Saathoff, H., Krämer, M., Mangold, A., Budz, P., Zink, P., Schreiner, J., Mauersberger, K., Haag, W., Kärcher, B., and Schurath, U.: Experimental investigation of homogeneous freezing of sulphuric acid particles in the aerosol chamber AIDA, *Atmos. Chem. Phys.*, 3, 211–223, doi:10.5194/acp-3-211-2003, 2003.
- 1030
- Murphy, D. M. and Koop, T.: Review of the vapour pressures of ice and supercooled water for atmospheric applications, *Q. J. R. Meteorol. Soc.*, 131, 1539–1565, doi:10.1256/qj.04.94, 2005.
- Murray, B. J., Broadley, S. L., Wilson, T. W., Atkinson, J. D., and Wills, R. H.: Heterogeneous freezing of water droplets containing kaolinite particles, *Atmos. Chem. Phys.*, 11, 4191–4207, doi:10.5194/acp-11-4191-2011, 2011.
- 1035
- Murray, B. J., O’Sullivan, D., Atkinson, J. D., and Webb, M. E.: Ice nucleation by particles immersed in supercooled cloud droplets, *Chem. Soc. Rev.*, 41, 6519–6554, doi:10.1039/C2CS35200A, 2012.
- Myhre, G., Shindell, D., Bréon, F.-M., Collins, W., Fuglestedt, J., Huang, J., Koch, D., Lamarque, J.-F., Lee, D., Mendoza, B., Nakajima, T., Robock, A., Stephens, G., T., T., and Zhang, H.: *Climate Change 2013: The Physical Science Basis. Contribution of Working Group I to the Fifth Assessment Report of the Intergovernmental Panel on Climate Change*, chap. 8. Anthropogenic and Natural Radiative Forcing, pp. 659–740, Cambridge University Press, Cambridge, United Kingdom and New York, NY, USA, 2013.
- 1040
- Niedermeier, D., Hartmann, S., Shaw, R. A., Covert, D., Mentel, T. F., Schneider, J., Poulain, L., Reitz, P., Spindler, C., Clauss, T., Kiselev, A., Hallbauer, E., Wex, H., Mildenerger, K., and Stratmann, F.: Heterogeneous freezing of droplets with immersed mineral dust particles measurements and parameterization, *Atmos. Chem. Phys.*, 10, 3601–3614, doi:10.5194/acp-10-3601-2010, 2010.
- 1045
- Niedermeier, D., Shaw, R. A., Hartmann, S., Wex, H., Clauss, T., Voigtländer, J., and Stratmann, F.: Heterogeneous ice nucleation: exploring the transition from stochastic to singular freezing behavior, *Atmos. Chem. Phys.*, 11, 8767–8775, doi:10.5194/acp-11-8767-2011, <http://www.atmos-chem-phys.net/11/8767/2011/>, 2011.
- 1050
- Niemand, M., Möhler, O., Vogel, B., Vogel, H., Hoose, C., Connolly, P., Klein, H., Bingemer, H., DeMott, P., Skrotzki, J., and Leisner, T.: A particle-surface-area-based parameterization of immersion freezing on desert dust particles, *J. Atmos. Sci.*, 69, 3077–3092, doi:10.1175/JAS-D-11-0249.1, 2012.
- 1055
- O’Sullivan, D., Murray, B. J., Malkin, T. L., Whale, T. F., Umo, N. S., Atkinson, J. D., Price, H. C., Baustian, K. J., Browse, J., and Webb, M. E.: Ice nucleation by fertile soil dusts: relative importance of mineral and biogenic components, *Atmos. Chem. Phys.*, 14, 1853–1867, doi:10.5194/acp-14-1853-2014, 2014.
- Park, K., Dutcher, D., Emery, M., Pagels, J., Sakurai, H., Scheckman, J., Qian, S., Stolzenburg, M. R., Wang, X., Yang, J., and McMurry, P. H.: Tandem measurements of aerosol properties-A review of mobility techniques with extensions, *Aerosol Sci. Technol.*, 42, 801–816, doi:10.1080/02786820802339561, 2008.
- 1060
- Pinti, V., Marcolli, C., Zobrist, B., Hoyle, C. R., and Peter, T.: Ice nucleation efficiency of clay minerals in the immersion mode, *Atmos. Chem. Phys.*, 12, 5859–5878, doi:10.5194/acp-12-5859-2012, 2012.

- Pruppacher, H. R. and Klett, J. D.: *Microphysics of Clouds and Precipitation*, Kluwer Academic Publishers, Netherlands, 1997.
- 1065 Riechers, B., Wittbracht, F., Hutten, A., and Koop, T.: The homogeneous ice nucleation rate of water droplets produced in a microfluidic device and the role of temperature uncertainty, *Phys. Chem. Chem. Phys.*, 15, 5873–5887, doi:10.1039/C3CP42437E, 2013.
- Rigg, Y. J., Alpert, P. A., and Knopf, D. A.: Immersion freezing of water and aqueous ammonium sulphate droplets initiated by Humic Like Substances as a function of water activity, *Atmos. Chem. Phys.*, 13, 4917–4961, doi:10.5194/acpd-13-4917-2013, 2013.
- 1070 Rogers, D. C., DeMott, P. J., Kreidenweis, S. M., and Chen, Y. L.: A continuous-flow diffusion chamber for airborne measurements of ice nuclei, *J. Atmos. Ocean. Technol.*, 18, 725–741, 2001.
- Rosenfeld, D., Andreae, M. O., Asmi, A., Chin, M., de Leeuw, G., Donovan, D. P., Kahn, R., Kinne, S., Kivekäs, N., Kulmala, M., Lau, W., Schmidt, K. S., Suni, T., Wagner, T., Wild, M., and Quaas, J.: Global observations of aerosol-cloud-precipitation-climate interactions, *Rev. Geophys.*, 52, 750–808, doi:10.1002/2013RG000441, 2014.
- 1075 Rossow, W. and Schiffer, R.: Advances in understanding clouds from ISCCP, *B. Am. Meteorol. Soc.*, 80, 2261–2287, doi:10.1175/1520-0477(1999)080<2261:AIUCFI>2.0.CO;2, 1999.
- Schill, G. P. and Tolbert, M. A.: Heterogeneous ice nucleation on phase-separated organic-sulfate particles: effect of liquid vs. glassy coatings, *Atmos. Chem. Phys.*, 13, 4681–4695, doi:10.5194/acp-13-4681-2013, 2013.
- 1080 Schmid, O., Karg, E., Hagen, D. E., Whitefield, P. D., and Ferron, G. A.: On the effective density of non-spherical particles as derived from combined measurements of aerodynamic and mobility equivalent size, *J. Aerosol Sci.*, 38, 431–443, doi:10.1016/j.jaerosci.2007.01.002, 2007.
- 1085 Slowik, J. G., Stainken, K., Davidovits, P., Williams, L. R., Jayne, J. T., Kolb, C. E., Worsnop, D. R., Rudich, Y., DeCarlo, P. F., and Jimenez, J. L.: Particle morphology and density characterization by combined mobility and aerodynamic diameter measurements. Part 2: Application to combustion-generated soot aerosols as a function of fuel equivalence ratio, *Aerosol Sci. Technol.*, 38, 1206–1222, doi:10.1080/027868290903916, 2004.
- 1090 Stetzer, O., Baschek, B., Luond, F., and Lohmann, U.: The Zurich Ice Nucleation Chamber (ZINC) - A new instrument to investigate atmospheric ice formation, *Aerosol Sci. Technol.*, 42, 64–74, 2008.
- Szakáll, M., Diehl, K., Mitra, S. K., and Borrmann, S.: A Wind Tunnel Study on the Shape, Oscillation, and Internal Circulation of Large Raindrops with Sizes between 2.5 and 7.5 mm, *J. Atmos. Sci.*, 66, 755–765, doi:10.1175/2008JAS2777.1, 2009.
- 1095 Tajiri, T., Yamashita, K., Murakami, M., Saito, A., Kusunoki, K., Orikasa, N., and Lilie, L.: A novel adiabatic-expansion-type cloud simulation chamber, *J. Meteorol. Soc. Jpn.*, 91, 687–704, doi:10.2151/jmsj.2013-509, 2013.
- Tao, W.-K., Chen, J.-P., Li, Z., Wang, C., and Zhang, C.: Impact of aerosols on convective clouds and precipitation, *Rev. Geophys.*, 50, doi:10.1029/2011RG000369, 2012.
- 1100 Tobo, Y., Prenni, A. J., DeMott, P. J., Huffman, J. A., McCluskey, C. S., Tian, G., Pöhlker, C., Pöschl, U., and Kreidenweis, S. M.: Biological aerosol particles as a key determinant of ice nuclei populations in a forest ecosystem, *J. Geophys. Res.*, 118, 10 100–10 110, doi:10.1002/jgrd.50801, 2013.

- Vali, G.: Quantitative evaluation of experimental results on heterogeneous freezing nucleation of supercooled liquids, *J. Atmos. Sci.*, 29, 402–409, doi:10.1175/1520-0469(1971)028<0402:QEOERA>2.0.CO;2, 1971.
- 1105 Vali, G.: Repeatability and randomness in heterogeneous freezing nucleation, *Atmos. Chem. Phys.*, 8, 5017–5031, doi:10.5194/acp-8-5017-2008, 2008.
- Vali, G. and Snider, J. R.: Time-dependent freezing rate parcel model, *Atmos. Chem. Phys.*, 15, 2071–2079, doi:10.5194/acp-15-2071-2015, 2015.
- Welti, A., Lüönd, F., Stetzer, F. O., and Lohmann, U.: Influence of particle size on the ice nucleating ability of mineral dusts, *Atmos. Chem. Phys.*, 9, 6705–6715, 2009.
- 1110 Welti, A., Lüönd, F., Kanji, Z. A., Stetzer, O., and Lohmann, U.: Time dependence of immersion freezing: an experimental study on size selected kaolinite particles, *Atmos. Chem. and Phys.*, 12, 9893–9907, doi:10.5194/acp-12-9893-2012, www.atmos-chem-phys.net/12/9893/2012/, 2012.
- Wex, H., DeMott, P. J., Tobo, Y., Hartmann, S., Rösch, M., Clauss, T., Tomsche, L., Niedermeier, D., and Stratmann, F.: Kaolinite particles as ice nuclei: learning from the use of different kaolinite samples and different coatings, *Atmos. Chem. Phys.*, 14, 5529–5546, doi:10.5194/acp-14-5529-2014, 2014.
- 1115 Wiedensohler, A. and Fissan, H. J.: Aerosol charging in high purity gases, *J. Aerosol Sci.*, 19, 867–870, doi:10.1016/0021-8502(88)90054-7, 1988.
- Wright, T. P. and Petters, M. D.: The role of time in heterogeneous freezing nucleation, *J. Geophys. Res.*, 118, 3731–3743, doi:10.1002/jgrd.50365, 2013.
- 1120 Zelenyuk, A., Cai, Y., and Imre, D.: From agglomerates of spheres to irregularly shaped particles: Determination of dynamic shape factors from measurements of mobility and vacuum aerodynamic diameters, *Aerosol Sci. Technol.*, 40, 197–217, doi:10.1080/02786820500529406, 2006.
- Zobrist, B., Koop, T., Luo, B. P., Marcolli, C., and Peter, T.: Heterogeneous ice nucleation rate coefficient of water droplets coated by a nonadecanol monolayer, *J. Phys. Chem. A*, 111, 2149–2155, doi:10.1021/jp066080w, 2007.
- 1125 Zuberi, B., Bertram, A., Cassa, C. A., Molina, L. T., and Molina, M. J.: Heterogeneous nucleation of ice in $(\text{NH}_4)_2\text{SO}_4\text{-H}_2\text{O}$ particles with mineral dust immersions, *Geophys. Res. Lett.*, 29, 10, 1504, doi:10.1029/2001GL014289, 2002.

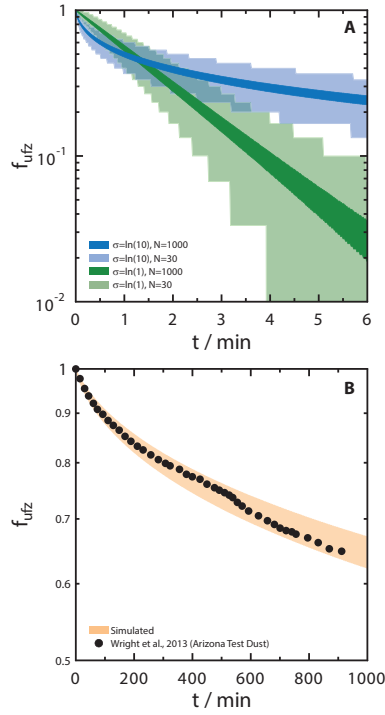


Figure 1. Sensitivity calculations of the unfrozen droplet fraction, f_{ufz} , as a function of time, t , derived from model simulations for a total number of droplets, N_{tot} , and variability of ice nuclei surface area, σ_g . **(a)** Model simulated 5 and 95% bounds of f_{ufz} are shown as dark green (Iso1), light green (Iso2), dark blue (Iso3), and light blue (Iso4) shading. Parameter values are given in the legend. **(b)** Simulated 5 and 95% bounds of f_{ufz} derived from IsoWR are shown as the orange shading along with experimental data of isothermal immersion freezing by Arizona test dust (Wright and Petters, 2013) shown as black circles. Parameter values for all model simulations in **(a)** and **(b)** are given in Table 1.

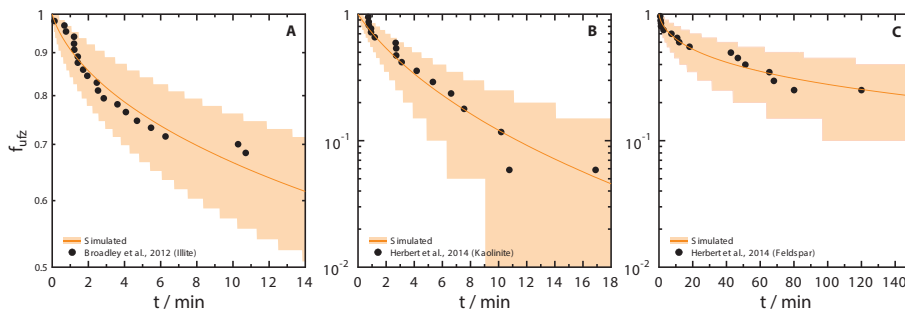


Figure 2. Simulated and experimentally (Broadley et al., 2012; Herbert et al., 2014) derived unfrozen droplet fractions, f_{ufz} , as a function of time, t . Model simulations and IN types used are: **(a)** IsoBR and illite, **(b)** IsoHE1 and kaolinite, and **(c)** IsoHE2 and feldspar, respectively. Orange lines and shading represent \bar{f}_{ufz} and corresponding 5 and 95% bounds, respectively. Parameter values for model simulations are given in Table 1.

Table 1. Summary of parameters used in isothermal model simulations.

Name	N_{tot}	σ_g	A_g / cm^2	T / K	J_{het} $\text{cm}^{-2} \text{s}^{-1}$	IN Type	Figure	Color
Iso1	1000	1	1.0×10^{-5}	–	1.0×10^3	–	1a	dark green
Iso2	30	1	1.0×10^{-5}	–	1.0×10^3	–	1a	light green
Iso3	1000	10	1.0×10^{-5}	–	1.0×10^3	–	1a	dark blue
Iso4	30	10	1.0×10^{-5}	–	1.0×10^3	–	1a	light blue
IsoWR	1000	9.5	6.4×10^{-3}	251.15	6.0×10^{-4}	ATD ^a	1b	orange
IsoBR	63	8.3	2.6×10^{-7}	243.3	1.3×10^3	illite	2a	orange
IsoHE1	40	2.2	1.2×10^0	255.15	4.1×10^{-3}	kaolinite	2b	orange
IsoHE2	40	8.5	2.0×10^{-2}	262.15	2.0×10^{-2}	feldspar	2c	orange
IsoDI1	45	4.2	5.1×10^{-1}	255.15	1.3×10^{-2}	illite	3	green
IsoDI2	45	9.1	5.1×10^{-2}	252.15	9.5×10^{-1}	illite	3	orange
IsoDI3	45	1.5	5.1×10^{-1}	252.15	8.3×10^{-1}	illite	3	blue
IsoCFDC	833	MCD ^b	MCD	238.65– 247.65 ^c	ABIFM ^d	kaolinite	7	blue, green
IsoLACIS	21	MCD	MCD	235.65– 238.65 ^c	ABIFM	kaolinite	7	orange, black

^a Arizona Test Dust.^b A multiple charge distribution (MCD) was used to define the surface area distribution. See text and Fig. S1 for further details.^c Isothermal simulations were performed at 0.15 K increments within the stated temperature range.^d Values of J_{het} are calculated from the water activity, a_w , based immersion freezing model (ABIFM) (Knopf and Alpert, 2013).**Table 2.** Summary of parameters used in cooling rate model simulations.

Name	N_{tot}	σ_g	A_g / cm^2	m	c	$r / \text{K min}^{-1}$	IN Type	Figure	Color
Cr1	1000	10	1.0×10^{-5}	54.48	–10.67	0.5	illite	4	orange
Cr2	1000	10	1.0×10^{-5}	54.48	–10.67	5.0	illite	4	blue
CrHE1	40	8.5	2.1×10^{-2}	122.83	–12.98	0.2	feldspar	5	orange
CrHE2	40	8.5	2.1×10^{-2}	122.83	–12.98	2.0	feldspar	5	blue
CrDI1	45	5.7	2.9×10^0	54.48	–10.67	non-linear ^a	illite	6	orange
CrDI2	45	5.7	2.9×10^{-2}	54.48	–10.67	non-linear ^a	illite	6	blue
		$A_{\text{tot}} / \text{cm}^2$	$D_{\text{p,g}} / \mu\text{m}$						
CrNI1	6.5×10^{-4}	1.72	0.42	22.91	–1.27	non-linear ^b	ND ^c	8	blue
CrNI2	5.4×10^{-4}	1.69	0.40	22.91	–1.27	non-linear ^b	ND ^c	8	orange
		N_{tot}							
MPC1	10^7	1	0.3	54.48	–10.67	0.36	illite	10	red
MPC2	10^7	5	0.3	54.48	–10.67	0.36	illite	10	blue

^a A continuous non-linear cooling rate with time is given in Diehl et al. (2014).^b A continuous non-linear cooling rate with time due to adiabatic expansion is fitted to experimental trajectories (Niemand et al., 2012) using a 4th order polynomial.^c Natural dusts from Niemand et al. (2012): Asian, Saharan, Israeli and Canary Island dust.

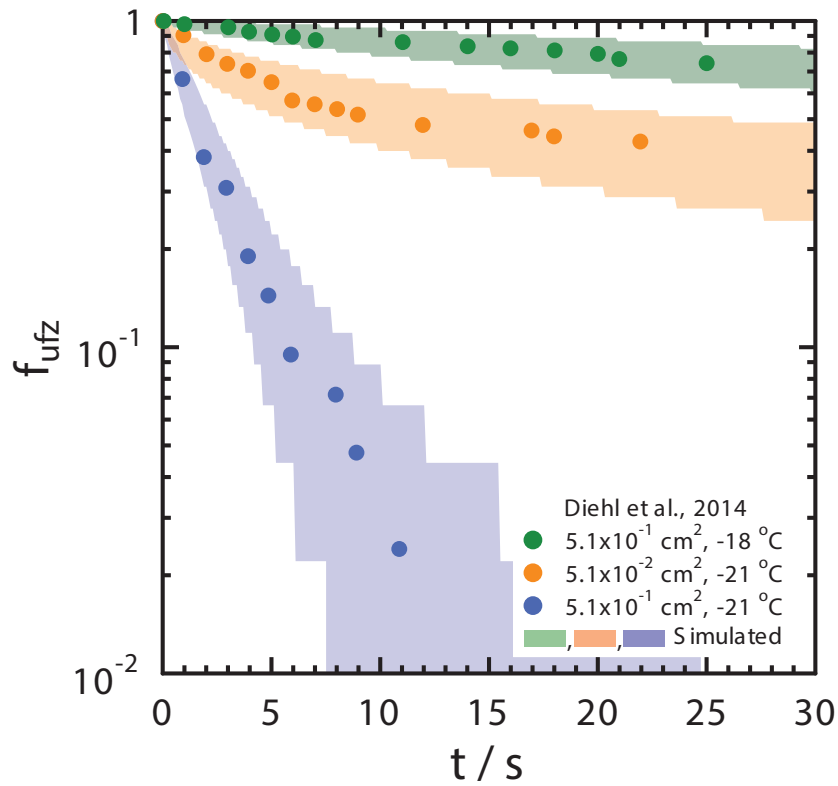


Figure 3. Simulated and experimentally (Diehl et al., 2014) derived unfrozen droplet fractions, f_{ufz} , as a function time, t , using illite. Model simulated 5 and 95% bounds of f_{ufz} are shown as green, orange and blue shading for IsoDI1, IsoDI2 and IsoDI3, respectively. Temperature and average surface area per droplet reported by Diehl et al. (2014) are given in the legend. Parameter values for model simulations are given in Table 1.

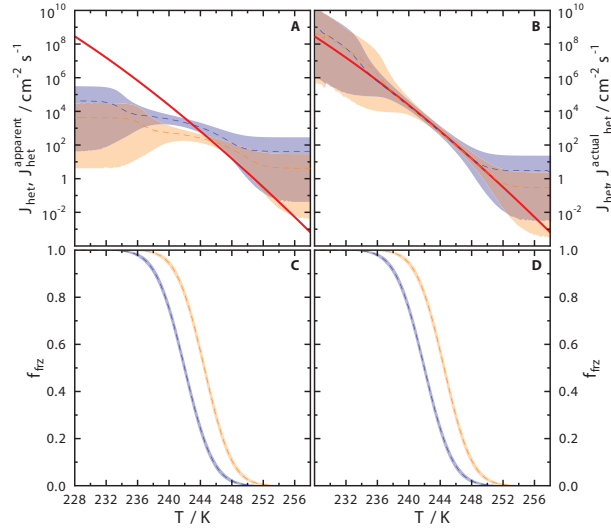


Figure 4. Sensitivity calculations of heterogeneous ice nucleation rate coefficients, J_{het} , and frozen droplet fractions, f_{frz} , on cooling rate, r , derived from model simulations Cr1 (orange) and Cr2 (blue) where $r = 0.5$ and 5.0 K min^{-1} , respectively. J_{het} as a function of temperature, T , are shown in (a) assuming uniform ice nuclei surface area (ISA) per droplet yielding $J_{\text{het}}^{\text{apparent}}$, and (b) accounting for different ISA yielding $J_{\text{het}}^{\text{actual}}$. The dashed lines in (a) and (b) are $\bar{J}_{\text{het}}^{\text{apparent}}$ and $\bar{J}_{\text{het}}^{\text{actual}}$, respectively. Shadings in (a) and (b) correspond to upper and lower fiducial limits with $x = 0.999$ confidence and the solid red line is calculated from Eq. (6) for illite (Knopf and Alpert, 2013). Frozen droplet fractions, f_{frz} , are shown in (c) and (d) where dashed lines and shadings represent \bar{f}_{frz} and 5 and 95% bounds, respectively. Parameter values for Cr1 and Cr2 are given in Table 2.

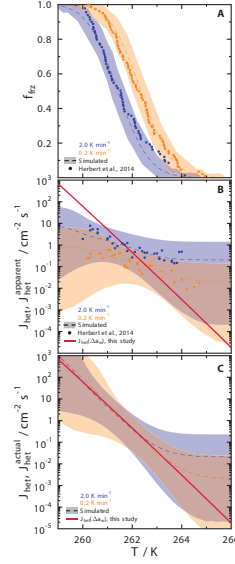


Figure 5. Frozen droplet fractions, f_{frz} , and heterogeneous ice nucleation rate coefficients, J_{het} , from immersion freezing cooling rate, r , dependent model simulations CrHE1 and CrHE2 where $r = 0.2$ (orange) and 2.0 K min^{-1} (blue), respectively, and experimental data of feldspar acting as immersion IN (Herbert et al., 2014). Dashed lines and shadings in **(a)** are \bar{f}_{frz} and 5 and 95% bounds, respectively. J_{het} as a function of temperature, T , are shown in **(b)** assuming uniform ice nuclei surface area (ISA) per droplet yielding $J_{\text{het}}^{\text{apparent}}$ and **(c)** accounting for variable ISA yielding $J_{\text{het}}^{\text{actual}}$. The dashed lines in **(b)** and **(c)** are $\bar{J}_{\text{het}}^{\text{apparent}}$ and $\bar{J}_{\text{het}}^{\text{actual}}$, respectively. Shadings in **(b)** and **(c)** correspond to upper and lower fiducial limits with $x = 0.999$ confidence. Experimentally derived f_{frz} and J_{het} are shown as circles in **(a)** and **(b)**, respectively (Herbert et al., 2014). The red line in **(b)** and **(c)** is calculated from Eq. (6) (Knopf and Alpert, 2013) using new parameters derived for feldspar. Parameter values for CrHE1 and CrHE2 are given in Table 2.

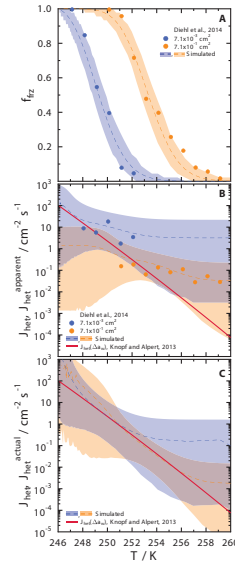


Figure 6. Frozen droplet fractions, f_{fz} , and heterogeneous ice nucleation rate coefficients, J_{het} , from immersion freezing model simulations CrDI1 (orange) and CrDI2 (blue), and experimental data of illite acting as immersion IN are shown (Diehl et al., 2014). Dashed lines and shadings in (a) are \bar{f}_{fz} and 5 and 95% bounds, respectively. J_{het} as a function of temperature, T , are shown in (b) assuming uniform ice nucleating particle surface area (ISA) per droplet yielding $J_{het}^{apparent}$ and (c) accounting for variable ISA yielding J_{het}^{actual} . The dashed lines in (b) and (c) are $\bar{J}_{het}^{apparent}$ and \bar{J}_{het}^{actual} , respectively. Shadings in (b) and (c) correspond to upper and lower fiducial limits with $x = 0.999$ confidence. Experimentally derived f_{fz} and J_{het} are shown as circles in (a) and (b), respectively (Diehl et al., 2014). The red line in (b) and (c) is calculated from Eq. (6) for illite (Knopf and Alpert, 2013). Parameter values for CrDI1 and CrDI2 are given in Table 2.

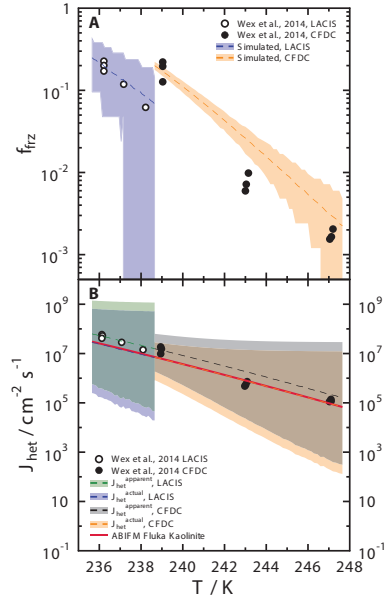


Figure 7. Frozen droplet fractions, f_{frz} , and heterogeneous ice nucleation rate coefficients, J_{het} , from isothermal model simulations IsoCFDC (orange and black) and IsoLACIS (blue and green), and experimental data of immersion freezing due to kaolinite by Wex et al. (2014) are shown. Dashed lines and shadings in (a) are \bar{f}_{frz} and 5 and 95% bounds, respectively. J_{het} as a function of temperature, T , are shown in (b) assuming uniform ice nucleating particle surface area (ISA) per droplet yielding $J_{\text{het}}^{\text{apparent}}$, and accounting for variable ISA yielding $J_{\text{het}}^{\text{actual}}$. The dashed lines in (b) are $\bar{J}_{\text{het}}^{\text{apparent}}$ and $\bar{J}_{\text{het}}^{\text{actual}}$ as indicated in the legend. Shadings in (b) correspond to upper and lower fiducial limits with $x = 0.999$ confidence and the red line is calculated from Eq. (6) for kaolinite (Knopf and Alpert, 2013). Parameter values for IsoCFDC and IsoLACIS are given in Table 1.

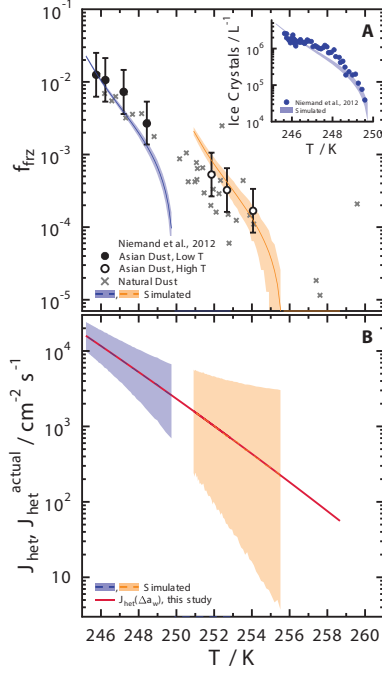


Figure 8. Frozen droplet fractions, f_{frz} , and heterogeneous ice nucleation rate coefficients, J_{het} , derived from adiabatic cooling immersion freezing model simulations CrNI1 (blue) and CrNI2 (orange). Simulated and experimentally observed ice crystal concentrations are shown in the insert of panel (a). Dashed lines and shadings in (a) are \bar{f}_{frz} and 5 and 95% bounds, respectively. Experimentally derived f_{frz} and uncertainties by Niemand et al. (2012) are shown as symbols and error bars. J_{het} as a function of temperature, T , is shown in (b) and accounting for variable ISA yielding $J_{\text{het}}^{\text{actual}}$, where dashed lines and shading are $\bar{J}_{\text{het}}^{\text{actual}}$ and fiducial limits with $x = 0.999$ confidence, respectively. The red line in (b) is calculated from Eq. (6) using new parameters derived for natural dust. Parameter values for CrNI1 and CrNI2 are given in Table 2.

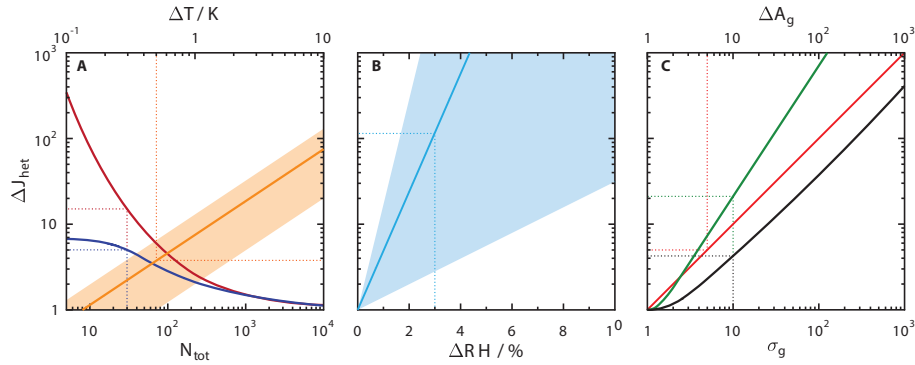


Figure 9. Uncertainty analysis derived from immersion freezing model simulations. The relative error in the experimentally derived heterogeneous ice nucleation rate coefficient, J_{het} , is referred to as ΔJ_{het} . The y axis indicates ΔJ_{het} as a factor error, e.g. $\Delta J_{\text{het}} = 10$ indicates an error in J_{het} by a factor of 10 in the positive and negative direction. stochastic error due to the applied number of droplets, N_{tot} , is shown in (a) where red and blue represent the upper and lower fiducial limits of J_{het} , respectively. The error due to temperature accuracy, ΔT , for a variety of IN types is shown in (a) in orange color where the solid line is average ΔJ_{het} as a function of ΔT and the shading is for a range of IN types. The error due to the absolute uncertainty in water activity or equivalently relative humidity, ΔRH , is shown in (b) where the blue line is average ΔJ_{het} , and the shading represents the range of values for a variety of IN types. The uncertainty due to variability in IN surface area, σ_g , is shown in (c) as black and green lines evaluated at $f_{\text{frz}} = 0.1$ and 0.9 , respectively. The uncertainty in measuring absolute surface area, ΔA_g , is shown in (c) as the red line. Further details and example uncertainty values given as dotted lines are described in the text.

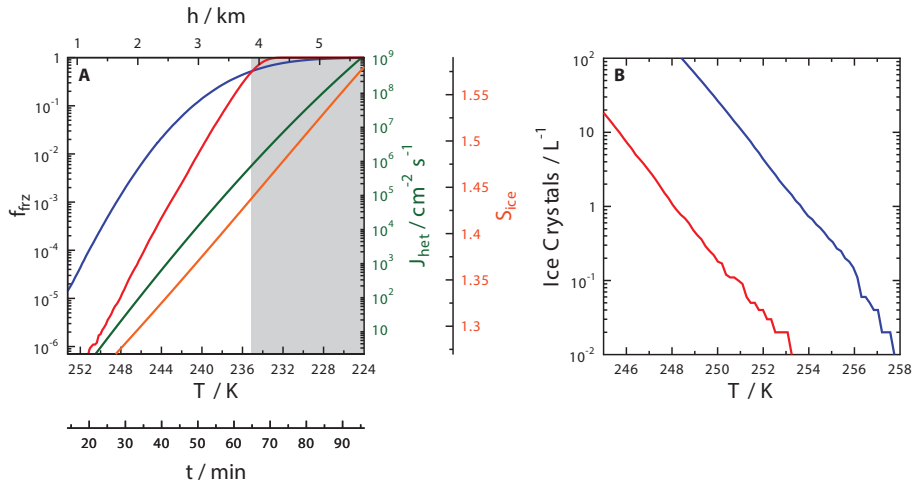


Figure 10. Results of two ice nucleation models for mixed-phase cloud conditions (MPC1 and MPC2) considering uniform ($\sigma_g = 1$) or lognormally ($\sigma_g = 5$) distributed IN diameters, D_p , respectively. Median D_p for both is 300 nm. Parameter values for MPC1 and MPC2 are given in Table 2. Immersion freezing is simulated for 10^7 particles in 100 L of air with an updraft velocity, $w = 100 \text{ cm s}^{-1}$ and a lapse rate, $\Gamma = 6 \text{ K km}^{-1}$. Frozen droplet fraction, f_{ice} , is shown in (a) as a function of temperature, T , time, t , and height, h , for MPC1 and MPC2 as red and blue lines, respectively. The green line is the heterogeneous ice nucleation rate coefficient, J_{het} , calculated using Eq. (6) for illite (Knopf and Alpert, 2013) and the orange line is the ice saturation ratio, S_{ice} . (b) Ice crystals per liter of air derived from MPC1 and MPC2 are given by the red and blue lines, respectively.